

HIV-1 Polymerase Inhibition by Nucleoside Analogs: Cellular- and Kinetic Parameters of Efficacy, Susceptibility and Resistance Selection

Max von Kleist^{1*}, Philipp Metzner², Roland Marquet³, Christof Schütte¹

1 Department of Mathematics and Computer Science, Free University Berlin, Berlin, Germany, **2** Institute of Computational Science, University of Lugano, Lugano, Switzerland, **3** Architecture et Réactivité de l'ARN, Université de Strasbourg, CNRS, IBMC, Strasbourg, France

Abstract

Nucleoside analogs (NAs) are used to treat numerous viral infections and cancer. They compete with endogenous nucleotides (dNTP/NTP) for incorporation into nascent DNA/RNA and inhibit replication by preventing subsequent primer extension. To date, an integrated mathematical model that could allow the analysis of their mechanism of action, of the various resistance mechanisms, and their effect on viral fitness is still lacking. We present the first mechanistic mathematical model of polymerase inhibition by NAs that takes into account the reversibility of polymerase inhibition. Analytical solutions for the model point out the cellular- and kinetic aspects of inhibition. Our model correctly predicts for HIV-1 that resistance against nucleoside analog reverse transcriptase inhibitors (NRTIs) can be conferred by decreasing their incorporation rate, increasing their excision rate, or decreasing their affinity for the polymerase enzyme. For all analyzed NRTIs and their combinations, model-predicted macroscopic parameters (efficacy, fitness and toxicity) were consistent with observations. NRTI efficacy was found to greatly vary between distinct target cells. Surprisingly, target cells with low dNTP/NTP levels may not confer hyper-susceptibility to inhibition, whereas cells with high dNTP/NTP contents are likely to confer natural resistance. Our model also allows quantification of the selective advantage of mutations by integrating their effects on viral fitness and drug susceptibility. For zidovudine triphosphate (AZT-TP), we predict that this selective advantage, as well as the minimal concentration required to select thymidine-associated mutations (TAMs) are highly cell-dependent. The developed model allows studying various resistance mechanisms, inherent fitness effects, selection forces and epistasis based on microscopic kinetic data. It can readily be embedded in extended models of the complete HIV-1 reverse transcription process, or analogous processes in other viruses and help to guide drug development and improve our understanding of the mechanisms of resistance development during treatment.

Citation: von Kleist M, Metzner P, Marquet R, Schütte C (2012) HIV-1 Polymerase Inhibition by Nucleoside Analogs: Cellular- and Kinetic Parameters of Efficacy, Susceptibility and Resistance Selection. *PLoS Comput Biol* 8(1): e1002359. doi:10.1371/journal.pcbi.1002359

Editor: Thomas Lengauer, Max-Planck-Institut für Informatik, Germany

Received: August 1, 2011; **Accepted:** December 5, 2011; **Published:** January 19, 2012

Copyright: © 2012 von Kleist et al. This is an open-access article distributed under the terms of the Creative Commons Attribution License, which permits unrestricted use, distribution, and reproduction in any medium, provided the original author and source are credited.

Funding: MvK acknowledges acknowledges financial support by the German Ministry of Education and Sciences (BMBF) and from the DFG research center MATHEON. PM acknowledges funding from the DFG research center MATHEON and DFG SPP 1276 (MetStröm). RM was supported by grants from Sidaction and ANRS (Agence Nationale de Recherches sur le SIDA et les Hépatites). The funders had no role in study design, data collection and analysis, decision to publish, or preparation of the manuscript.

Competing Interests: The authors have declared that no competing interests exist.

* E-mail: vkleist@zedat.fu-berlin.de

Introduction

Viral encoded polymerases perform essential enzymatic steps through amplification- or transformation of the viral genome during the viral life cycle [1]. As such, viral encoded polymerases constitute an attractive drug target for the treatment of many viral infections [2]. Nucleoside analogs (NAs) were among the first polymerase inhibitors that showed *clinical* efficacy [3–5] and are nowadays broadly used to treat hepatitis B-, herpes simplex- and HIV-1 infection [2], where they constitute the typical backbone components of modern highly active antiretroviral treatment (HAART). Nucleoside analogs are typically formulated as pro-drugs, which require intracellular phosphorylation to form an analog of (deoxy-) nucleoside-triphosphate (NA-TP; mimicking either adenosine, thymidine, guanine, cytosine or uracil), which can be incorporated into nascent viral DNA by the viral polymerase. After incorporation, nucleoside analogs bring the polymerization machinery to a halt, as they lack the chemical

group that is necessary to attach the next incoming nucleotide [6]. Incorporated NAs can, however, be selectively excised by some viral polymerases, rescuing the nascent viral DNA and inducing a transient-, rather than permanent mode of inhibition. Inhibition of the crucial step of viral DNA polymerization can lower the probability by which circulating virus can successfully infect host cells [7] and the number of viral progeny produced per unit time, shifting the balance between viral clearance by the immune system and viral replication in favor of the immune system. For the ease of notation, we will subsequently only refer to the active (triphosphorylated) nucleoside analog moiety.

Inhibition of DNA polymerization by NAs is not restricted to viral polymerase, but can also affect cellular polymerases, leading to unwanted side-effects [8,9]. The therapeutic window of NAs largely depends on molecular kinetic properties of the respective enzymes with regard to a particular inhibitor [10,11]. NAs therefore require high specificity for the targeted viral enzyme to allow for a clinical benefit. Viral resistance development can revert

Author Summary

Nucleoside analogs (**NAs**) represent an important drug class for the treatment of viral infections and cancer. They inhibit DNA/RNA polymerization after being incorporated into nascent DNA/RNA, which prevents primer extension. Viruses are particularly versatile and frequently develop mutations enabling them to avert the effects of **NAs**. The mechanisms of resistance development are, however, still poorly understood. Through mathematical modeling, we assess the mechanisms by which HIV-1 can develop resistance against nucleoside analog reverse transcriptase inhibitors (NRTI). We quantify the effects of treatment and estimate the fitness of drug resistant mutants. We correctly predict that HIV-1 can develop resistance by decreasing NRTI incorporation rate, increasing its excision rate, or decreasing its affinity for the viral polymerase enzyme. Our model also allows quantification of the cell specific factors affecting NRTI efficacy. Resistance development also changes drug susceptibility distinctly and we show, for the first time, that selection of drug resistance can occur in particular target cells. This finding could provide an explanation of how *clinically* observed resistant viral mutants may arise. It also pin-points important parameters that may impact clinical efficacy of **NAs** used to treat other viruses.

this specificity by changing the kinetic properties of the viral enzyme [12,13]. While a number of enzymatic studies have revealed crucial insights into the mechanisms of polymerase inhibition by **NAs** and the kinetic consequences of resistance development, an integrated mathematical insight into these mechanisms has rarely been achieved. In this study, we aim to mathematically formulate a model of polymerase inhibition by **NAs**, by integrating available enzymatic knowledge. The derived mathematical model should subsequently allow us to assess the impact of distinct cellular- and molecular determinants of **NA** inhibition and to achieve a greater understanding of viral resistance development and epistatic interactions. Results will be exemplified for inhibition of DNA polymerization during reverse transcription (RT) of HIV-1 by nucleoside analog reverse transcriptase inhibitors (NRTIs).

Initial mathematical modelling efforts in the context of RT inhibition by NRTIs of HIV-1 were based on the assumption that incorporation of chain-terminating nucleoside analogs is permanent [14]. The effect of NRTIs was therefore solely explained by their incorporation probability. In subsequent years after the introduction of zidovudine (AZT; the first NRTI against HIV-1), resistant strains were detected which displayed increased removal kinetics of AZT from terminated primers [15–17], rather than discriminating between the natural nucleotide and AZT [18]. This indicated that nucleoside analog removal is very significant and constitutes a major resistance pathway against thymidine analogs (like AZT) and many other NRTIs [13]. The particular mechanism of resistance to AZT indicated that chain termination by nucleoside analogs may not be permanent. Hence, a distinct view on polymerase inhibition by NRTIs is necessary, which departs from the assumption of permanent chain termination. Subsequent modeling work [19] used lumped kinetic expressions and Monte-Carlo simulations instead of deriving analytical expressions, which precludes the identification of key molecular determinants of efficacy and drug resistance. Both previous mathematical modeling efforts were not able to compute the fitness loss associated with mutations in the RT enzyme, an

important determinant in clinical settings and for studying epistatic interactions [20–23].

In this work, we present a distinct view of viral polymerase inhibition by NRTIs, which departs from the assumption of permanent chain termination. We propose that NRTIs delay the process of DNA polymerization, rather than permanently terminating it, simultaneously keeping in mind that any delay of the process decreases the number of viral progeny and the likelihood of target cell infection by the virus. The developed mathematical formulation allows us to study viral polymerase inhibition by NRTIs as well as fitness effects related to drug resistance development. By integrating fitness effects and drug susceptibility, it is further possible to quantify the selective pressure exerted by NRTIs and to study epistasis. The derived analytical expressions can be used to study the effects of single- and multiple NRTIs on DNA polymerization in the absence and presence of resistance mutations and can be useful for drug design. Chain termination by **NAs** may also be reversible in other viruses [24–26], against which **NAs** are being developed. Hence, the model may also be applicable to study **NA** inhibition of these viruses.

Results

Mechanism of action of nucleoside analogs on DNA polymerization

A schematic view of the process of viral DNA polymerization in the presence of **NAs** is illustrated in Fig. 1. We interpret the process of DNA polymerization as a Markov jump process with $2 \cdot N - 1$ states (Fig. 1A), where each state in the model corresponds to the number of incorporated nucleosides: state ‘0’ corresponds to the initiation of polymerization, states $i = 1 \dots N$ in the model correspond to the condition in which i nucleosides have been attached and state ‘ N ’ corresponds to the final polymerization product. States \bar{i} correspond to the condition, in which the DNA-chain consists of $i - 1$ natural nucleosides, but where the last (i th) molecule in the chain is a chain-terminating nucleoside analog.

At each state i , the nascent DNA-chain can either be shortened (pyrophosphorolysis reaction r_{pyro}), -prolonged with a nucleoside (polymerase reaction r_{pol}) or -terminated by a nucleoside analog (reaction r_{term}). If the chain has been terminated (state $\bar{i} + 1$), it can get released with rate r_{exc} (excision reaction) to produce a chain of length i . The kinetics of these reactions will be detailed later.

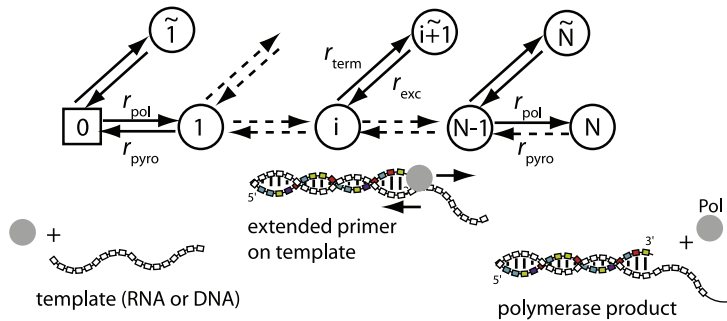
Taking into account the mode of action of chain terminating nucleoside analogs, we conclude that polymerization will be decelerated in the presence of these inhibitors, because the overall time required to go from state ‘0’ (initiation of polymerization) to state ‘ N ’ (final polymerization product) in Fig. 1 will be prolonged in their presence by introducing ‘waiting states’ \bar{i} . The residual polymerase activity of the wildtype enzyme in the presence of activated (tri-phosphorylated) nucleoside analogs ($1 - \varepsilon(\text{NA}, \text{wt})$) can thus be expressed as:

$$1 - \varepsilon(\text{NA}, \text{wt}) = \frac{T_{0 \rightarrow N}(\phi, \text{wt})}{T_{0 \rightarrow N}(\text{NA}, \text{wt})} \quad (\text{inhibition of wildtype}), \quad (1)$$

where $T_{0 \rightarrow N}(\phi, \text{wt})$ and $T_{0 \rightarrow N}(\text{NA}, \text{wt})$ denote the expected time to finalize DNA polymerization in the wildtype ‘wt’ in the absence of drugs ‘ ϕ ’ and in the presence of active nucleoside analogs **NA** respectively.

Analogously, we can define the effect of chain terminating nucleoside analogs on some viral mutant, $1 - \varepsilon(\text{NA}, \text{mut})$ and the fitness loss associated with some mutant in the absence of treatment ϕ , $f(\text{mut})$:

A Model of DNA/RNA polymerization in the presence of NAs



B Sequence Context

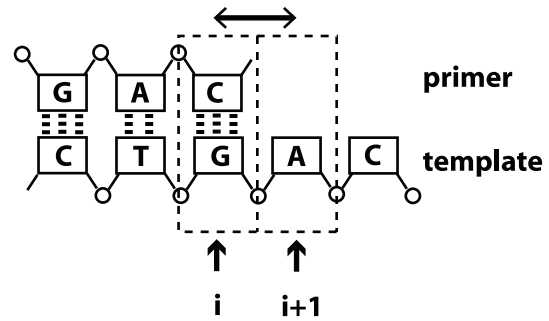


Figure 1. DNA-polymerization in the presence of chain terminating nucleoside analogs. A: The mathematical model defines a Markov jump process: Each state in the model corresponds to the number of incorporated nucleotides: state '0' corresponds to the polymerase enzyme binding to the template, prior to polymerization, states $i = 1 \dots N$ in the model correspond to the condition in which i nucleosides have been attached and state ' N ' corresponds to full-length product, after which the enzyme dissociates from the template/primer. States $i+1$ correspond to the condition, in which a DNA-chain consisting of i natural nucleosides has been produced, but where the last ($i+1$)th nucleoside in the chain is a chain-terminating NA. At each state i , the nascent DNA-chain can either be shortened (pyrophosphorolysis r_{pyro}), -prolonged with a nucleoside (polymerase reaction r_{pol}) or -terminated by a nucleoside analog (reaction r_{term}). If the chain has been terminated (state $i+1$), it can get released with rate r_{exc} (excision reaction) to produce a chain of length i . B: Sequence context. The reaction rates r_{pol} , r_{pyro} , r_{term} and r_{exc} depend on the nucleoside sequence of the template. In the illustration, the next incoming nucleoside could be either a thymidine or a thymidine-analog (corresponding to position $i+1$ in the template sequence). Therefore, $r_{pol}(i+1)$ and $r_{term}(i+1)$ would refer to thymidine- and thymidine-analog incorporation. The pyrophosphorolysis reaction, on the other hand, would refer to cytosine removal (position i in the primer sequence). doi:10.1371/journal.pcbi.1002359.g001

$$1 - \varepsilon(\text{NA, mut}) = \frac{T_{0 \rightarrow N}(\phi, \text{mut})}{T_{0 \rightarrow N}(\text{NA, mut})} \quad (\text{inhibition of mutant}) \quad (2)$$

$$f(\text{mut}) = \frac{T_{0 \rightarrow N}(\phi, \text{wt})}{T_{0 \rightarrow N}(\phi, \text{mut})} \quad (\text{fitness of mutant}). \quad (3)$$

These constituents can be seen as building blocks for describing the fitness landscape of any arbitrary viral mutant 'mut' in the absence- and presence of inhibitors, see e.g. [7,27].

Based on the definitions above, we can also assess the combined effects of selection and drug pressure for any viral strain, i.e. $f(\text{mut}) \cdot (1 - \varepsilon(\text{NA, mut}))$. This allows us to assess the selective advantage $S_{\text{mut/wt}}(\text{NA})$ of a mutant viral strain over the wild type in an environment that is pharmacologically modified by NAs.

$$\begin{aligned} S_{\text{mut/wt}}(\text{NA}) &= \frac{f(\text{mut}) \cdot (1 - \varepsilon(\text{NA, mut}))}{(1 - \varepsilon(\text{NA, wt}))} \\ &= \frac{T_{0 \rightarrow N}(\text{NA, wt})}{T_{0 \rightarrow N}(\text{NA, mut})} \quad (\text{selective advantage}) \end{aligned} \quad (4)$$

This parameter integrates the (usually opposed) effects of mutations on resistance and viral fitness. If $S_{\text{mut/wt}}(\text{NA}) < 1$, the wild type virus is selected over the mutant strain, whereas $S_{\text{mut/wt}}(\text{NA}) > 1$ indicates selection of a mutant virus over the wild type. Since $S_{\text{mut/wt}}(\text{NA})$ depends on the concentration of NAs, a critical concentration of nucleoside analog $\text{NA}^*(\text{mut})$ can exist, above which the selection of a particular viral strain over the wild type is favored. $S_{\text{mut1/mut2}}(\text{NA}) = \frac{T_{0 \rightarrow N}(\text{NA, mut2})}{T_{0 \rightarrow N}(\text{NA, mut1})}$ can also be used to assess selection between two arbitrary mutant strains mut1 and mut2 in a pharmacologically modified environment.

Finally, we can assess epistatic interactions for combinations of mutations with regard to viral replication. Briefly, in a two-locus-two-allele model, epistasis is positive if some double mutant m12 replicates better than expected from the single mutants m1 and m2, normalized by the replication of the wild type wt (background). Epistasis is negative if the replication of the double mutant is less than expected from the single mutants. Along the same lines, epistasis has been used to study interactions of mutations in the absence of drugs [22] and for escalating drug concentrations [23]. Using the definitions above, in the presence of NAs, we derive:

$$\begin{aligned} E_{\text{Rep}}(\text{NA}) &= \log((1 - \varepsilon(\text{NA, mut12})) \cdot f(\text{mut12}) \cdot (1 - \varepsilon(\text{NA, wt})) \cdot f(\text{wt})) \\ &\quad - \log((1 - \varepsilon(\text{NA, mut1})) \cdot f(\text{mut1}) \cdot (1 - \varepsilon(\text{NA, mut2})) \cdot f(\text{mut2})). \end{aligned} \quad (5)$$

The equation above becomes positive if the first term is greater than the second, i.e. the double mutant replicates better than expected from the single mutants, in agreement with the definition of epistasis [22,23]. The epistasis term $E_{\text{Rep}}(\text{NA})$ defined above regards both fitness effects and drug resistance. In the absence of drugs, $(1 - \varepsilon) = 1$, see eqs. (1)–(2) above, we get the fitness epistasis:

$$\begin{aligned} E_f(\phi) &= \log(f(\text{mut12}) \cdot f(\text{wt})) - \log(f(\text{mut1}) \\ &\quad \cdot f(\text{mut2})) \quad (\text{fitness epistasis}) \end{aligned} \quad (6)$$

It is also possible to only analyze epistatic effects on resistance:

$$\begin{aligned} E_{\text{Res}}(\text{NA}) &= \log((1 - \varepsilon(\text{NA, mut12})) \cdot (1 - \varepsilon(\text{NA, wt}))) \\ &\quad - \log((1 - \varepsilon(\text{NA, mut1})) \cdot (1 - \varepsilon(\text{NA, mut2}))) \end{aligned} \quad (7)$$

(resistance epistasis).

Note, that the defined terms are additive, i.e. $E_{\text{Rep}}(\text{NA}) = E_f(\phi) + E_{\text{Res}}(\text{NA})$.

Polymerization of Hetero-Polymeric sequences

The process of DNA polymerization (Fig. 1) defines a birth-death process. We are interested in the derivation of an explicit formula for the *mean first passage time* $T_{0 \rightarrow N}$ (the average time required to finalize DNA polymerization). Let $T_{i \rightarrow i+1}$ denote the expected time required to extend the DNA-chain by one nucleoside (going from state i to state $i+1$, derivation see eq (22)–(28); Methods section)

$$T_{i \rightarrow i+1} = (\tau_{i+1} \cdot \rho_{i \rightarrow i+1} + \tau_i + \rho_{i \rightarrow i-1} T_{i-1 \rightarrow i}) \frac{1}{\rho_{i \rightarrow i+1}}. \quad (8)$$

where τ_i, τ_{i+1} are the waiting times in states i and $i+1$ respectively and $\rho_{i \rightarrow i+1}, \rho_{i \rightarrow i-1}$ are the probabilities to jump from state i to state $i+1$ and to state $i-1$ respectively. The parameter $\rho_{i \rightarrow i+1}$ denotes the probability that the chain of length i gets terminated by incorporation of a nucleoside analog (state $i+1$). The waiting times τ and jump-probabilities ρ are defined as follows:

$$\tau_i = \frac{1}{r_{\text{pol}}(i+1) + r_{\text{pyro}}(i) + r_{\text{term}}(i+1)}, \quad \tau_{i+1} = \frac{1}{r_{\text{exc}}(i+1)}, \quad (9)$$

$$\rho_{i \rightarrow i+1} = r_{\text{pol}}(i+1) \cdot \tau_i, \quad \rho_{i \rightarrow i-1} = r_{\text{pyro}}(i) \cdot \tau_i, \quad \rho_{i \rightarrow i+1} = r_{\text{term}}(i+1) \cdot \tau_i,$$

where $r_{\text{pol}}(i+1)$ and $r_{\text{term}}(i+1)$ denote the polymerase- and chain terminating reactions (attachment of the next incoming nucleoside or its analog), which depend on the efficacy of incorporation of the respective types of nucleosides (deoxyadenosine, -thymidine, -guanine or -cytosine triphosphate) or their respective analogs at position $i+1$ in the primer, see Fig. 1B. The parameter $r_{\text{exc}}(i+1)$ denotes the rate of release (excision reaction) of a primer that has been terminated at position $i+1$ by NA. The parameter $r_{\text{pyro}}(i)$ denotes the pyrophosphorolysis reaction, i.e. the rate at which a nucleoside is removed from the end of the primer. Note, that τ and ρ depend on the sequence context because the rates of nucleoside attachment and -removal depend on the types of nucleosides (and -analogs) to be incorporated and -removed respectively (see e.g. Fig. 1B). Eq. (8) allows us to calculate the time to finalize polymerization recursively, using the relation:

$$T_{0 \rightarrow N} = \sum_{i=0}^{N-1} T_{i \rightarrow i+1}. \quad (10)$$

If $i=0$ corresponds to the unextended primer, we have $r_{\text{pyro}}(0)=0$ in eq. (9) and therefore eq. (8) simplifies to

$$T_{0 \rightarrow 1} = (\tau_1 \cdot \rho_{0 \rightarrow 1} + \tau_0) \frac{1}{\rho_{0 \rightarrow 1}}, \quad (11)$$

with $\tau_0 = \frac{1}{r_{\text{pol}}(1) + r_{\text{term}}(1)}, \tau_1 = \frac{1}{r_{\text{exc}}(1)}$ and $\rho_{0 \rightarrow 1} = r_{\text{pol}}(1) \cdot \tau_0, \rho_{0 \rightarrow 1} = r_{\text{term}}(1) \cdot \tau_0$, which can be used as a recursion start to compute the polymerization time.

In the case where no chain-terminating inhibitor is applied, we have $r_{\text{term}}(i)=0$ for all i in eq. (9) and therefore eq. (8), and eqs. (10)–(11) simplify accordingly.

Eq. (8)–(10) can subsequently be used to estimate the residual polymerase activity in the presence of NAs in the wild type and any mutant enzyme, using eq. (1) and eq. (2) respectively, to estimate the fitness of some mutant with regard to polymerization, using eq. (3), or to estimate the selective advantage of a viral strain

against a competitor, using eq. (4). This will be exemplified in the next section.

Sequence dependent DNA-polymerization in the presence of NAs. Using eq. (10), it is possible to compute the average polymerization time ($T_{0 \rightarrow i}$) in the absence- and presence of NAs for any arbitrary sequence to be polymerized. In this section, we motivate the use of this approach and show how key phenotypic characteristics can be derived from this simple mathematical model.

NAs compete with the natural nucleoside substrates for the same binding site on the polymerase enzyme. We therefore take into account competitive inhibition for the kinetics of nucleoside- and nucleoside analog incorporation.

$$r_{\text{term}} = \frac{k_{\text{term}} \cdot [\text{NA}]}{K_{\text{D,NA}} \left(1 + \frac{[\text{dNTP}]}{K_{\text{D,dNTP}}} \right) + [\text{NA}]} \quad (12)$$

$$r_{\text{pol}} = \frac{k_{\text{pol}} \cdot [\text{dNTP}]}{K_{\text{D,dNTP}} \left(1 + \frac{[\text{NA}]}{K_{\text{D,NA}}} \right) + [\text{dNTP}]} \quad (13)$$

where $[\text{dNTP}]$ is the concentration of the deoxynucleoside triphosphates (adenosine-, thymidine-, cytidine- and guanosine-) of which the NA is an analog of. The variable $[\text{NA}]$ denotes the concentrations of activated (tri-phosphorylated) nucleoside analog that competes with its natural nucleoside counterpart for incorporation into the nascent viral DNA. The parameters k_{term} and k_{pol} denote the catalytic rate constants for incorporation of the NA and the dNTP respectively. $K_{\text{D,NA}}$ and $K_{\text{D,dNTP}}$ denote the dissociation constants for NA and dNTP binding to the polymerase respectively. In the absence of inhibitors ϕ , we have $[\text{NA}] = 0$ and therefore eq. (13) and eq. (12) simplify accordingly:

$$r_{\text{pol}}(\phi) = \frac{k_{\text{pol}} \cdot [\text{dNTP}]}{K_{\text{D,dNTP}} + [\text{dNTP}]}, \quad (14)$$

$$r_{\text{term}}(\phi) = 0. \quad (15)$$

Physiological dNTP concentrations for the most important target cell types of HIV-1 are indicated in Table 1. Parameters for natural nucleoside DNA- and RNA- dependent polymerization by wild type HIV-1 reverse transcriptase (RT) are indicated in Table S1 (supplementary material). In the forthcoming example, we will analyze the effect of a chain-terminating adenosine analog (ddATP, the active metabolite of didanosine, ddI) at a fixed concentration on both single nucleotide incorporation $T_{i \rightarrow i+1}$ (see eq. (8)) and on cumulative nucleoside polymerization $T_{0 \rightarrow i}$ (see eq. (10)) for physiological dNTP concentrations in resting CD4⁺ T-cells (Table 1). Furthermore, we will assess how polymerization is impaired by the (clinically relevant) ‘K65R’ mutation in reverse transcriptase in the absence- and presence of ddATP.

In Fig. 2 we have computed the average polymerization time for a short sequence (indicated on the x-axis in Fig. 2) and typical parameters for DNA-dependent polymerization for HIV-1 RT, see Table 1 and Table S1 (supplementary material). In this example, we have assumed that $r_{\text{pyro}} = r_{\text{exc}} = 0.0016 \text{ s}^{-1}$ [17] for all dNTP and for ddATP respectively. We examine polymerization in the absence- or the presence of 1.45 μM intracellular ddATP. The solid black line denotes the polymerization time in

Table 1. Physiological dNTP levels in different cell types.

	activated CD4 ⁺ -cells	resting CD4 ⁺ -cells	macrophages	ref.
dATP	5.1	1.7	0.023	[34]
dTTP	7.9	1.5	0.019	[34]
dCTP	5.9	1.9	0.03	[34]
dGTP	4.5	1.7	0.032	[34]
PPi	79	8	7	[35]
ATP	1400	2200	1600	[35]

All values are expressed in μM .
doi:10.1371/journal.pcbi.1002359.t001

the wild type RT in the absence of ddATP, whereas the blue dashed- and the red dotted lines indicate the polymerization time in the presence of ddATP in the wild type and drug-resistant mutant enzyme (bearing the 'K65R' mutation) respectively. The fold changes in the kinetic parameters, induced by the 'K65R' mutation, are stated in Table S2 (supplementary material). In the wild type enzyme the predicted incorporation probability $\rho_{i \rightarrow i+1}$ for ddATP over dATP is 9.4% in the presence of $1.45 \mu\text{M}$ ddATP. For the 'K65R' mutant $\rho_{i \rightarrow i+1}$ it is 3.2%. In Fig. 2A one can see the cumulative time to form the polymerization product $T_{0 \rightarrow i}$. In the presence of ddATP, the cumulative polymerization time is substantially increased (dashed blue line), which is partly compensated in the drug resistant enzyme bearing the 'K65R' mutation (dotted red line). In Fig. 2B we show the single nucleoside polymerization time $T_{i \rightarrow i+1}$. It can be seen, that in the presence of ddATP the single nucleoside polymerization time

$T_{i \rightarrow i+1}$ is substantially elevated, in relation to the wild type, whenever the respective natural nucleoside (here adenosine) needs to be incorporated (the solid black line vs. the dashed blue line). In the 'K65R' mutant (red dotted line), this is partially compensated for. However, in the mutant, the single nucleoside polymerization time $T_{i \rightarrow i+1}$ for incorporation of other nucleosides is also increased, which indicates, that the 'K65R' mutant might decrease the fitness of the enzyme. We have calculated the fitness of the mutant enzyme, the residual polymerase activity in the wild type enzyme -and the 'K65R' mutant and the selective advantage of the 'K65R' mutant over the wild type for the presented example, using eqs (1)–(4). The derived values are stated in Table 2. It can be seen that the 'K65R' mutant decreases ddATP inhibition of DNA dependent polymerization substantially (the residual polymerization is increased from 3.3% to 22.3%). However, the predicted fitness of the enzyme (in terms of DNA-dependent polymerization) is reduced to 37.9%. The predicted selective advantage of the 'K65R' mutant is 2.55, indicating that the 'K65R' resistance would be selected over the wild type in the presence of $1.45 \mu\text{M}$ ddATP.

Note, that in this section, we have exemplified the effects of a particular NA on polymerization, given a specific concentration of the respective NA and certain kinetic attributes of the polymerase enzyme (wild type RT vs. 'K65R' mutant RT). In the next sections, we will assess the general impact of certain resistance mechanisms, by analyzing a range of kinetic parameters and we will also study the efficacy of NAs for different concentration ranges.

Molecular determinants of inhibition

While in a hetero-polymeric sequence context, polymerase inhibition by NAs depends on the *particular* succession of the

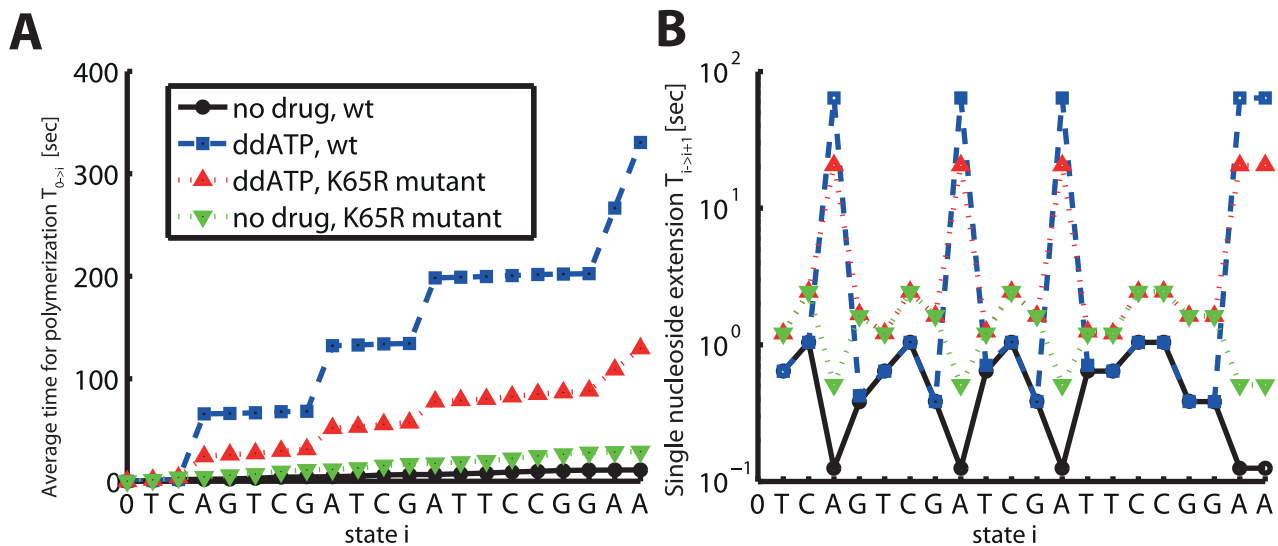


Figure 2. DNA-dependent polymerization of a hetero-polymeric sequence by HIV-1 RT in the presence- and absence of a chain terminating adenosine analog (ddATP). A: Cumulative time for polymerization of a hetero-polymeric sequence in the presence of a chain-terminating nucleoside analog (ddATP). The solid black line (filled dots) indicates the cumulative polymerization time up to sequence position i (the sequence position is indicated at the x-axis) in the absence of inhibitors in the wild type enzyme (calculated using eq. (10)). The dashed blue line (open squares) indicates the time required for polymerization in the presence of $1.45 \mu\text{M}$ ddATP. The dotted red- and green lines (upward and downward pointing triangles) show the time required for polymerization in the 'K65R' mutant RT enzyme in the presence- and absence of $1.45 \mu\text{M}$ ddATP. Kinetic parameters are presented in Table 1 and Table S1, S2 (supplementary material) for the wild type and the 'K65R' mutant. B: Single nucleoside incorporation time $T_{i \rightarrow i+1}$ in the absence of ddATP in the wildtype and the 'K65R' mutant (solid black and dashed green lines respectively) and in the presence of ddATP in the wild type enzyme (dashed blue line) and in the mutant enzyme (dotted red line), calculated using equation eq. (8).
doi:10.1371/journal.pcbi.1002359.g002

Table 2. Efficacy & fitness.

$1 - \varepsilon(\text{ddATP, wt})$	3.31%
$1 - \varepsilon(\text{ddATP, K65R})$	22.3%
$f'(\text{K65R})$	37.9%
$S_{\text{K65R/wt}}(\text{ddATP})$	2.55

Residual DNA-dependent polymerase activity ($1 - \varepsilon$) of HIV's RT in resting CD4⁺ T-cells in the presence of 1.45 μM ddATP and fitness (f') and selective advantage $S_{\text{K65R/wt}}$ with regard to DNA polymerization for the 'K65R' mutant. Calculations are based on formulas (1)–(4). doi:10.1371/journal.pcbi.1002359.t002

nucleosides, see e.g. Fig. 2B, this is not the case for homo-polymeric sequences, which consist of only one type of nucleoside, e.g. poly-adenosine; 'Poly-A'. This allows us to derive a general, analytical expression for polymerase inhibition by NAs, which is valid for *any* homo-polymeric sequence. We will make use of this fact to highlight key determinants of inhibition. For assessing the impact of nucleoside analogs in a *particular* hetero-polymeric sequence context, we advise to use eqs. (8)–(11). In a homo-polymeric sequence, we have $r_{\text{pol}}(i) \equiv r_{\text{pol}}, r_{\text{pyro}}(i) \equiv r_{\text{pyro}}, r_{\text{term}}(i) \equiv r_{\text{term}}$ and $r_{\text{exc}}(i) \equiv r_{\text{exc}}$ for all i . In this particular case, the explicit solution for the *mean first passage time* $T_{0 \rightarrow N}$ reads (see eq. (31)–(32); Methods section)

$$T_{0 \rightarrow N}(\text{NA}) = \left(\frac{r_{\text{term}} + r_{\text{exc}}}{r_{\text{exc}}} \right) \frac{(r_{\text{pol}} + r_{\text{pyro}})^{N-1} + r_{\text{pol}}^{N-1} \cdot (N-1)}{r_{\text{pol}}^N}. \quad (16)$$

When no inhibitor is present (ϕ), we have $r_{\text{term}} = 0$ and thus eq. (16) simplifies accordingly:

$$T_{0 \rightarrow N}(\phi) = \frac{(r_{\text{pol}}(\phi) + r_{\text{pyro}})^{N-1} + r_{\text{pol}}(\phi)^{N-1} \cdot (N-1)}{r_{\text{pol}}(\phi)^N}, \quad (17)$$

where r_{pol} and $r_{\text{pol}}(\phi)$ are the polymerization rates in the presence and absence (ϕ) of a competing NA, given in eq. (13) and eq. (14). Recalling the effect of NAs on polymerization, see eq. (1), we can derive the **residual polymerase activity** during NA treatment on a **homo-polymeric sequence**, $(1 - \eta) = \frac{T_{0 \rightarrow N}(\phi)}{T_{0 \rightarrow N}(\text{NA})}$:

$$(1 - \eta) = \frac{r_{\text{exc}}}{r_{\text{term}} + r_{\text{exc}}} \frac{r_{\text{pol}}^N}{r_{\text{pol}}(\phi)^N} \cdot \left(\frac{(r_{\text{pol}}(\phi) + r_{\text{pyro}})^{N-1} + r_{\text{pol}}(\phi)^{N-1} \cdot (N-1)}{(r_{\text{pol}} + r_{\text{pyro}})^{N-1} + r_{\text{pol}}^{N-1} \cdot (N-1)} \right) \quad (18)$$

The above expression simplifies further, if the pyrophosphorolysis reaction is very inefficient relative to polymerization, which is the case for most viral polymerase enzymes; e.g. $r_{\text{pyro}} \ll r_{\text{pol}} \leq r_{\text{pol}}(\phi)$.

$$(1 - \eta) \approx \frac{r_{\text{exc}}}{\underbrace{r_{\text{term}} + r_{\text{exc}}}_{\text{incorporation \& termination}}} \cdot \frac{r_{\text{pol}}}{\underbrace{r_{\text{pol}}(\phi)}_{\text{binding competition}}} \quad (19)$$

Eq. (19) highlights the two distinct mechanisms by which inhibition can be conferred, namely a) inhibitor incorporation (and subsequent quasi-termination of the polymerization reaction) and

b) competition for binding with natural nucleoside substrates. The efficacy of quasi-termination of the nascent DNA chain depends on the efficacy of inhibitor incorporation r_{term} and the duration of the chain termination, determined by r_{exc} . Binding competition is solely determined by the fractional decrease of the natural polymerization reaction (relative to the absence of inhibitor), see eq. (13).

After substituting the enzymatic rate expressions eqs. (12)–(14) into equation (19), we can solve for the fifty percent inhibitory concentration IC_{50} (see eqs. (33)–(35); Methods section), which refers to polymerase inhibition in a homo-polymeric sequence (e.g. 'Poly-A') and to the intracellular concentration of activated (triphosphorylated) NA.

$$\text{IC}_{50} \approx \frac{r_{\text{exc}}}{k_{\text{term}} + r_{\text{exc}}} \cdot K_{\text{D,NA}} \left(1 + \frac{[\text{dNTP}]}{K_{\text{D,dNTP}}} \right) \quad (20)$$

The above equation highlights the processes, which determine the efficacy of a chain-terminating nucleoside analog, namely the kinetic constants $k_{\text{term}}, K_{\text{D,NA}}$ and $K_{\text{D,dNTP}}$, the concentration of natural nucleoside $[\text{dNTP}]$ and the excision rate of the inhibitor r_{exc} .

Cell-specific susceptibility to chain-terminating nucleoside analogs. Viruses can infect numerous activated- and resting cells. HIV-1, for example, has been shown to infect activated- and resting CD4⁺ T-cells, macrophages, dendritic cells, natural killer cells and microglial cells [28–32], and possibly many more. It is important to understand- and take into account heterogeneous- or cell specific drug efficacy, as it may be a primary source of residual viral replication and subsequent resistance development during treatment [33].

In the context of nucleoside analog efficacy, the major cell-specific factors (apart from pharmacokinetics), are cell type-, or cell stage specific dNTP pools (see Table 1) and possibly cell specific rates of excision r_{exc} . In Fig. 3A, we predicted the impact of cell-specific $[\text{dNTP}]$ contents on DNA-dependent polymerization during HIV-1 reverse transcription in the presence of ddATP, using typical kinetic parameters (see Table S1, supplementary material).

Under the parameters used, a 100 fold increase in dNTP concentrations would result in a 19 fold increase in the IC_{50} value ($2.8 \cdot 10^{-3}$ vs. $5.3 \cdot 10^{-2} \mu\text{M}$), whereas a 100-fold decrease in the dNTP concentrations would only result in a 1.2 fold reduction in the IC_{50} value. This is an important observation, because it indicates that cells that contain high concentrations of dNTP can confer natural resistance against NRTIs, whereas cells with low dNTP content, like macrophages [34], do not necessarily confer hypersusceptibility to NRTIs. This phenomenon can be explained from eq. (20): The IC_{50} value does not decrease, if $[\text{dNTP}] \ll K_{\text{D,dNTP}}$.

Resting cells on the other hand might insufficiently phosphorylate NRTIs and subsequently contain lower levels of activated compound. However, these cells do not simultaneously require smaller NRTI concentrations for inhibition (IC_{50} value in Fig. 3A does not decrease with decreasing dNTP levels). Therefore, resting cells could constitute reservoirs for residual replication during antiviral treatment, if NRTI phosphorylation/activation is affected.

Excision of nucleoside reverse transcriptase inhibitors (NRTIs) of HIV-1 from terminated primers has been shown to be mediated by pyrophosphate (PPi) and ATP dependent mechanisms [35]. Whereas ATP concentrations are fairly similar in activated- and resting lymphocytes, as well as macrophages and monocytes [34–38] (1 to 5 mM), PPi levels have been shown to vary substantially

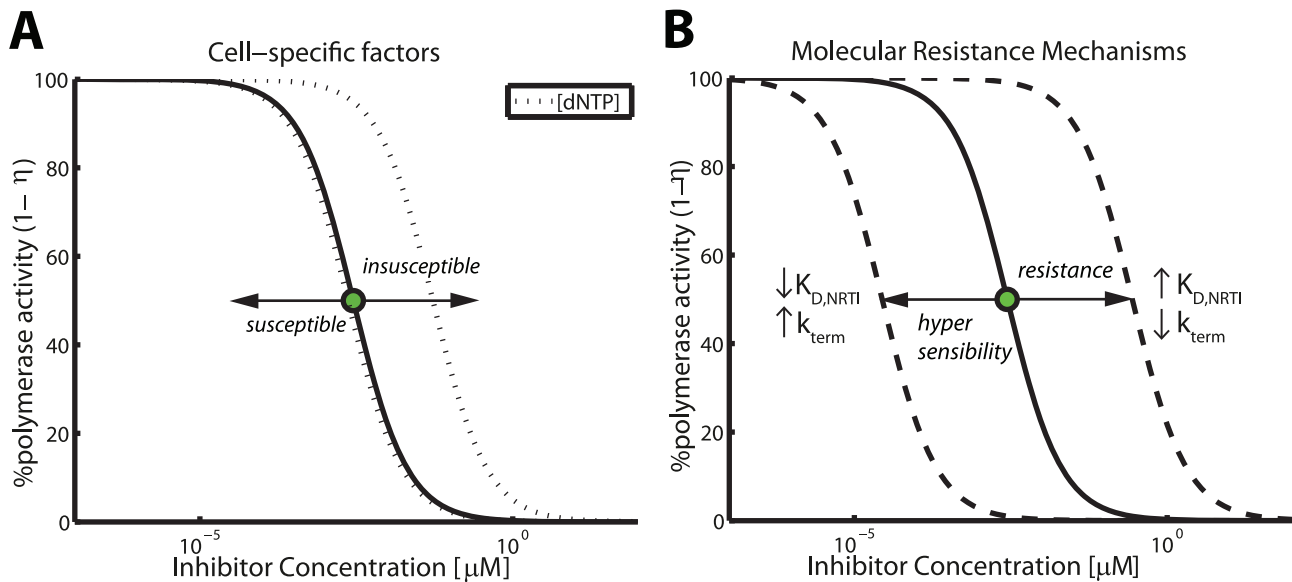


Figure 3. Factors that modify inhibition of DNA polymerization by nucleoside analogs. A: Cell-specific factors: Concentration response curve of ddATP for wild type RT during DNA-dependent polymerization (homo-polymeric sequence) in unstimulated CD4⁺ T-cells (solid line) and the impact of a 100-fold variation of the intracellular nucleoside concentrations (dotted line). The illustration was generated by evaluating eq. (19) and typical parameters for DNA-dependent polymerization during HIV-1 reverse transcription and its inhibition by ddATP (all parameters are indicated in Table 1 and Table S1, supplementary material). The corresponding IC₅₀ is depicted by a green filled circle. B: Molecular mechanisms of drug resistance and hyper-susceptibility (dashed lines). Impact of (i) selective attrition of inhibitor incorporation ($\downarrow k_{\text{term}}$) and (ii) selective attrition of inhibitor binding to the primer-template ($\uparrow K_{\text{D,NA}}$) on drug susceptibility. Hypersusceptibility is conferred by the opposite change in the indicated parameters. In order to generate the dashed lines, the respective parameters have been increased/decreased by a factor of 100. doi:10.1371/journal.pcbi.1002359.g003

[35] (8–80 μM), see also Table 1. This indicates that IC₅₀ values for polymerase inhibition by NAs might be cell-specific and may in some cells lead to incomplete suppression. Here, we did not analyze the effect of cell-specific PPi and ATP contents, as the kinetic parameters were not readily available for ddATP. We however discuss their impact on polymerase inhibition by zidovudine (AZT) in a subsequent section.

Molecular mechanisms of viral drug resistance against chain-terminating nucleoside analogs. The enzymatic properties of a viral polymerase can be adapted in an evolutionary process to counteract inhibition by NAs. Eq. (20) indicates that the following three distinct molecular mechanisms are likely to induce selective resistance against chain-terminating NAs, and indeed these three mechanisms of resistance have been described for HIV-1 RT [13].

- selective attrition of inhibitor incorporation ($\downarrow k_{\text{term}}$)
- selective attrition of inhibitor binding to the primer-template ($\uparrow K_{\text{D,NA}}$)
- enhanced excision of the NA from the terminated primer ($\uparrow r_{\text{exc}}$, by e.g. increasing the catalytic efficacy of removal or by increasing phosphate-donor, e.g. PPi- or ATP- binding).

The consequences of mutational modification of inhibitor incorporation (k_{term}) and -binding ($K_{\text{D,NA}}$) with regard to the predicted efficacy of ddATP are illustrated in Fig. 3B, where we have used typical parameters for DNA-dependent polymerization during HIV-1 reverse transcription (see Table S1, supplementary material). Under the utilized parameters a 100-fold change in the respective parameter k_{term} or $K_{\text{D,NRTI}}$ leads to a 100-fold change in the compounds IC₅₀ value. We did not analyze the effect of enhanced NA excision in Fig. 3B, as the kinetic parameters were not readily available for ddATP. These effects will be discussed in

the context of polymerase inhibition by zidovudine (AZT) in the next section.

Mechanism of zidovudine (AZT) resistance by thymidine analog mutations (TAMs)

It has been argued [17], that the main mechanism of AZT resistance is due to increased excision of AZT-MP from the terminated primer. In particular, this process has been shown to be both pyrophosphate- (PPi) and ATP- dependent *in vivo* [35]. For the rate of excision r_{exc} we can therefore write

$$r_{\text{exc}} = \frac{k_{\text{ATP}} \cdot [\text{ATP}]}{K_{\text{D,ATP}} + [\text{ATP}]} + \frac{k_{\text{PPi}} \cdot [\text{PPi}]}{K_{\text{D,PPi}} + [\text{PPi}]} \quad (21)$$

The variables [ATP] and [PPi] in the above equation refer to the concentration of adenosine triphosphate and pyrophosphate and the parameters k_{ATP} and k_{PPi} denote the catalytic rate constants for (ATP- and PPi dependent) excision. Parameters $K_{\text{D,ATP}}$ and $K_{\text{D,PPi}}$ denote the corresponding dissociation constants. The respective concentrations of PPi and ATP in various cell types are shown in Table 1 and kinetic parameters for AZT-MP excision during DNA- and RNA dependent polymerization by HIV-1 RT (wild type and AZT-resistant mutant) are indicated in Table S3 (supplementary material).

Residual polymerization in the presence of AZT. In Fig. 4, we have illustrated the predicted concentration-response relationship for intracellular AZT triphosphate and RNA- and DNA dependent polymerization of homo-polymeric- (panels A & B) and hetero-polymeric sequences in unstimulated CD4⁺ T-cells for the wild type enzyme (solid blue lines) and an AZT-resistant quadruple mutant ('D67N/K70R/T215Y/K219Q'; dashed lines), respectively. From Fig. 4, several conclusions can be drawn: First,

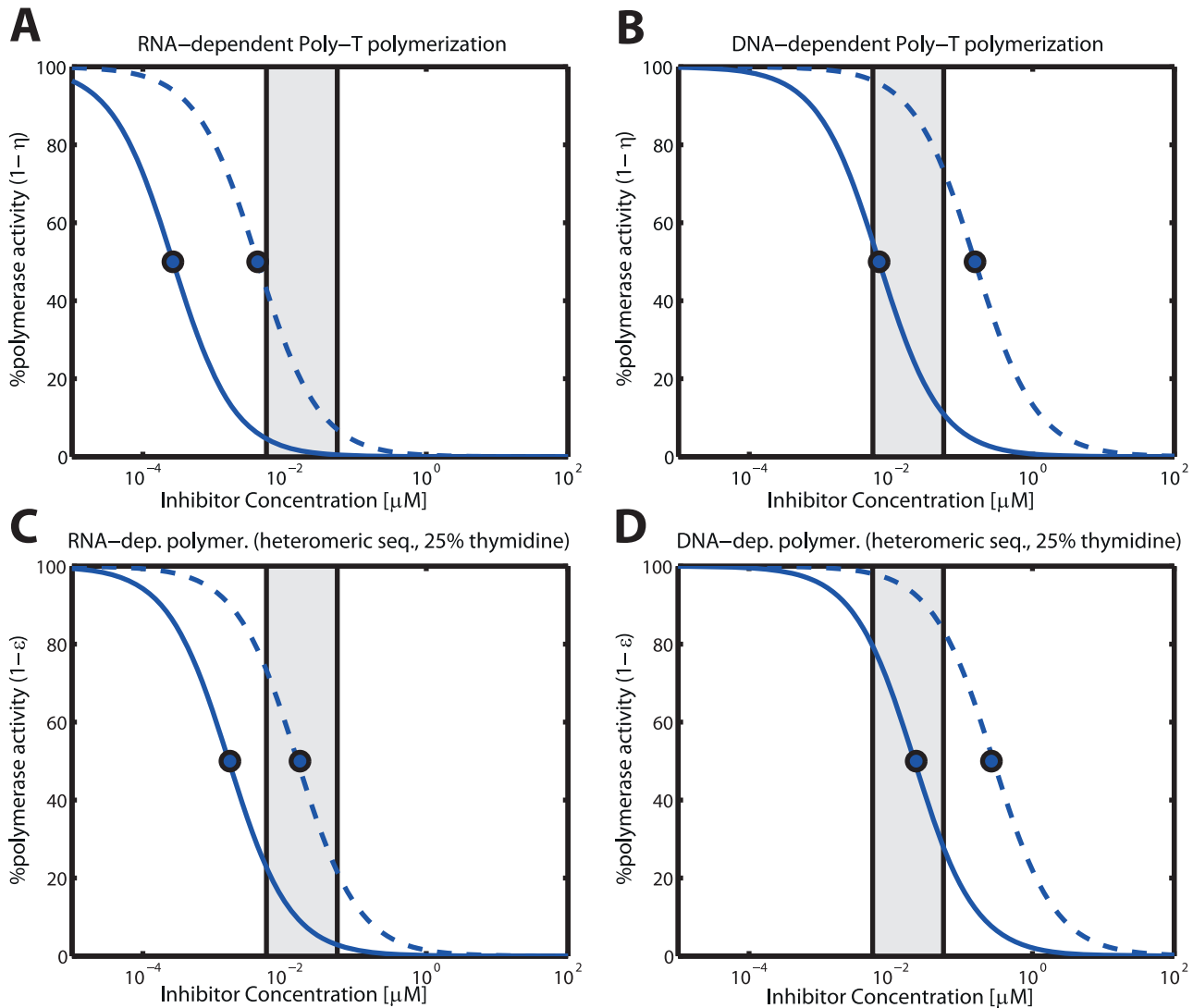


Figure 4. RNA- and DNA-dependent polymerization in the presence of intracellular AZT triphosphate in unstimulated CD4⁺ T-cells.

The solid blue curves indicate the level of residual polymerization with the wild type enzyme, whereas the dashed lines indicate the residual polymerization with the 'D67N/K70R/T215Y/K219Q' mutant. Panels A & B: Residual RNA- and DNA dependent polymerization of a homo-polymeric thymidine sequence (Poly-T). Calculations were obtained by solving eq. (19). Panels C & D: RNA- and DNA polymerization of a hetero-polymeric random sequence of length 500 with 25% respective dNTP content. The illustration was generated using eq. (10). The light grey area indicates the *in vivo* concentrations range of AZT in purified circulating CD4⁺ T-cells from [71], converted to units μM by assuming a cell volume of $180\mu\text{m}^3$ for resting CD4⁺ T-cells [72]. All utilized parameters are indicated in Tables 1, S1, S2, S3 (supplementary material). doi:10.1371/journal.pcbi.1002359.g004

as expected, polymerase inhibition by intracellular AZT is more efficient in homo-polymeric sequences that contain only thymidine versus hetero-polymeric sequences that contain a mixture of all four nucleosides (panel A & B vs. C & D). Second, AZT inhibition of RNA-dependent polymerization is more efficient than inhibition of DNA-dependent polymerization (panels A & C vs. panels B & D). Predicted inhibition of RNA-dependent polymerization of hetero-polymeric sequences is nearly complete for the wild type and under *in vivo* intracellular AZT-TP concentrations (residual activity is $\leq 20\%$, solid blue line and grey area in Fig. 4C). For DNA-dependent polymerization, we predict residual activity under *in vivo* AZT-TP concentrations ($\geq 20\%$, solid blue line and grey shaded area in Fig. 4D). Third, the resistance mutations 'D67N/K70R/T215Y/K219Q' (dotted lines) increase the fifty percent inhibitory AZT-TP concentrations.

For DNA-dependent polymerization, the IC_{50} is shifted to concentrations that lie beyond clinically achieved concentrations (see Fig. 4B & Fig. 4D), almost completely diminishing inhibition by AZT (Fig. 4D). RNA-dependent polymerization is still partially inhibited in the 'D67N/K70R/T215Y/K219Q' mutant in unstimulated CD4⁺ T-cells ($\geq 20\%$ residual polymerization, Fig. 4A & Fig. 4C).

Cell type specific susceptibility to AZT and impact of resistance. In Table 3, we have calculated the cell-specific IC_{50} values for RNA- and DNA dependent polymerization of homo-polymeric (Poly-'T') sequences. Our results indicate that AZT is much more potent in resting cells (unstimulated CD4⁺ T-cells and macrophages), as suggested by the smaller IC_{50} values for the wildtype in Table 3 (second- and fifth column). This cell-specific property is mainly due to lower PPI concentrations in resting cells

(see Table 1) and subsequently lesser pyrophosphorolysis of AZT-MP terminated primers in resting cells (see eqs. (20)–(21)) as discussed previously (section *Cell-specific susceptibility to chain-terminating nucleoside analogs*), and is only marginally affected by lower dNTP levels in resting cells, as decreasing dNTP levels may not induce hyper-susceptibility as shown in Fig. 3A. The greatest kinetic change induced by the ‘D67N/K70R/T215Y/K219Q’ affects the catalytic rate of ATP-mediated excision of AZT-MP from the terminated primer k_{ATP} (see Table S3, supplementary material). This change increases the predicted IC_{50} of AZT in unstimulated CD4^+ cells and macrophages in a much more pronounced way than in activated CD4^+ T-cells (fold resistance >15 in unstimulated CD4^+ T-cells and macrophages vs. <5 in activated CD4^+ T-cells; fourth and seventh columns in Table 3). In activated T-cells PPI-mediated excision of AZT-MP from the terminated primer is likely the dominant mechanism, as a consequence of the much higher PPI concentrations in these cells (see Table 1). Therefore, increasing k_{ATP} will only have a strong effect once ATP-mediated excision becomes the dominant mechanism of AZT-removal. Therefore, further increase of k_{ATP} might turn ATP-mediated excision into the main removal pathway and subsequently impact on resistance in a more pronounced way in activated CD4^+ cells as well. Overall, the IC_{50} for polymerase inhibition in the ‘D67N/K70R/T215Y/K219Q’ mutant is probably shifted into concentration ranges which are rarely achieved *in vivo*.

Molecular mechanism of AZT-resistance by ATP-mediated excision. Excision of AZT-MP from the terminated primer is the major mechanism by which AZT resistance is thought to be mediated [17]. In particular, ATP-mediated excision has been discussed as the major *in vivo* mechanism of AZT resistance [15,16]. However, at the molecular level, it is unclear, if the mechanism by which enhanced excision is achieved is due to an increased removal rate (parameter k_{ATP} in eq. (21)) or increased binding affinity of ATP to the primer-template (affected parameter: $K_{\text{D,ATP}}$ in eq. (21)). In particular, in a recent paper [39], it was argued, based on crystal structures of resistant RT, that the main mechanism of AZT-resistance could be conferred by increasing ATP’s binding affinity to the resistant RT enzyme. In Fig. 5, we analyze the impact of the two potential AZT-resistance mechanisms (increased removal rate k_{ATP} vs. decreased $K_{\text{D,ATP}}$). Our predictions show that increasing the affinity for ATP binding $K_{\text{D,ATP}}$ (dashed red line) does not lead to resistance development under the parameters used, because ATP binding to the wild type enzyme is already

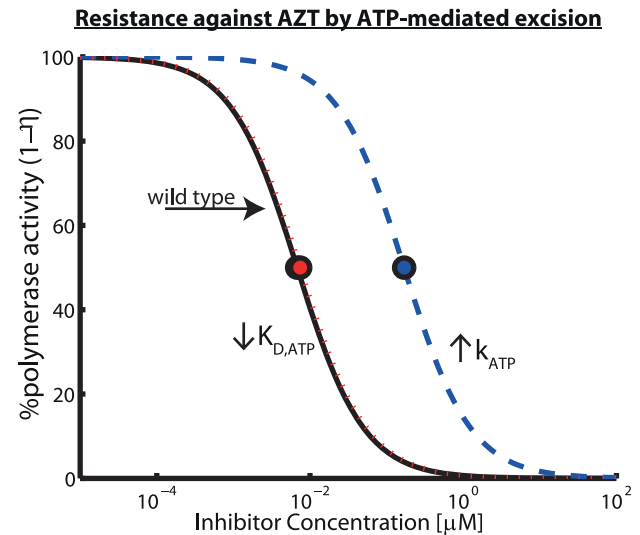


Figure 5. Molecular mechanisms of HIV-1 resistance development against AZT by ATP-mediated excision. Potential mechanisms for resistance development against AZT through increasing its excision rate r_{exc} via an ATP-mediated mechanism (see eq. (21)). We calculated residual DNA-dependent polymerization of a Poly-T sequence in unstimulated CD4^+ T-cells using eq. (19) with parameters from Tables 1, S1 and S3 (supplementary material). The solid black line shows residual DNA polymerization $(1-\eta)$ in the wild type virus, whereas the dotted red line and the dashed blue line refer to residual polymerization if $K_{\text{D,ATP}}$ and k_{ATP} were decreased- and increased 100-fold respectively.
doi:10.1371/journal.pcbi.1002359.g005

saturated ($K_{\text{D,ATP}} < [\text{ATP}]$) at physiological conditions and further decrease of $K_{\text{D,ATP}}$ enhances the saturation effect. However, increasing the removal rate k_{ATP} (dashed blue line) desensitizes reverse transcriptase-mediated polymerization to AZT inhibition since $r_{\text{exc}} \approx k_{\text{ATP}}$, in cells with low PPI contents and under saturation conditions (see Table 1 and eq. (21)).

Selection of resistance

Selection of drug resistance depends on the competitive advantage of some resistant mutant over its competitors (either the wild type or some competing viral mutant) in a particular environment. In order to quantify whether drug resistant mutants become selected in an environment that is modified by NAs, we have previously defined the selective advantage S in eq. (4) (and paragraph below).

Selection of thymidine associated mutations (TAMs) by AZT in different cell-types. In Fig. 6A and Fig. 6B, the selective advantage of TAMs over the wild type $S_{\text{TAM/wt}}(\text{AZT-TP})$ is shown for RNA-dependent polymerization (panel A) and DNA-dependent polymerization (panel B) respectively in distinct cell-types relevant to HIV-1 infection (solid green-, blue and red lines indicate $S_{\text{TAM/wt}}(\text{AZT-TP})$ for activated CD4^+ T-cells, resting CD4^+ T-cells and macrophages, respectively). The respective threshold concentrations AZT^* (TAM) above which resistance becomes selected, $S_{\text{TAM/wt}}(\text{AZT-TP}) > 1$, are $5.4 \cdot 10^{-4} \mu\text{M}$ (resting CD4^+ cells) $< 6.3 \cdot 10^{-4} \mu\text{M}$ (macrophages) $< 7.3 \cdot 10^{-3} \mu\text{M}$ (activated CD4^+ cells) for RNA-dependent polymerization. For DNA-dependent polymerization, the corresponding thresholds are $6.2 \cdot 10^{-3} \mu\text{M}$ (macrophages) $< 0.01 \mu\text{M}$ (resting CD4^+ cells) $< 0.36 \mu\text{M}$ (activated CD4^+ cells).

Table 3. Cell-specific IC_{50} values of AZT-TP for ‘poly-thymidine’ polymerization and susceptibility change by resistance development.

cell type	RNA/DNA		DNA/DNA			
	‘wt’	‘res’*	fold res.	‘wt’	‘res’*	fold res.
act. CD4^+	$2.4 \cdot 10^{-3}$	$1 \cdot 10^{-2}$	4.5	$6.6 \cdot 10^{-2}$	$2.7 \cdot 10^{-1}$	4.1
rest. CD4^+	$2.7 \cdot 10^{-4}$	$4.2 \cdot 10^{-3}$	15.7	$6.8 \cdot 10^{-3}$	$1.5 \cdot 10^{-1}$	22.6
macr.	$2.3 \cdot 10^{-4}$	$3.9 \cdot 10^{-3}$	17.2	$5.4 \cdot 10^{-3}$	$1.2 \cdot 10^{-1}$	22.5

IC_{50} values, expressed in μM , were calculated using eqs. (20)–(21). Cell-specific parameters were taken from Table 1. All kinetic parameters were taken from Table 1 and Tables S1, S2, S3 (supplementary material).

*‘res’ = D67N/K70R/T215Y/K219Q mutant.

doi:10.1371/journal.pcbi.1002359.t003

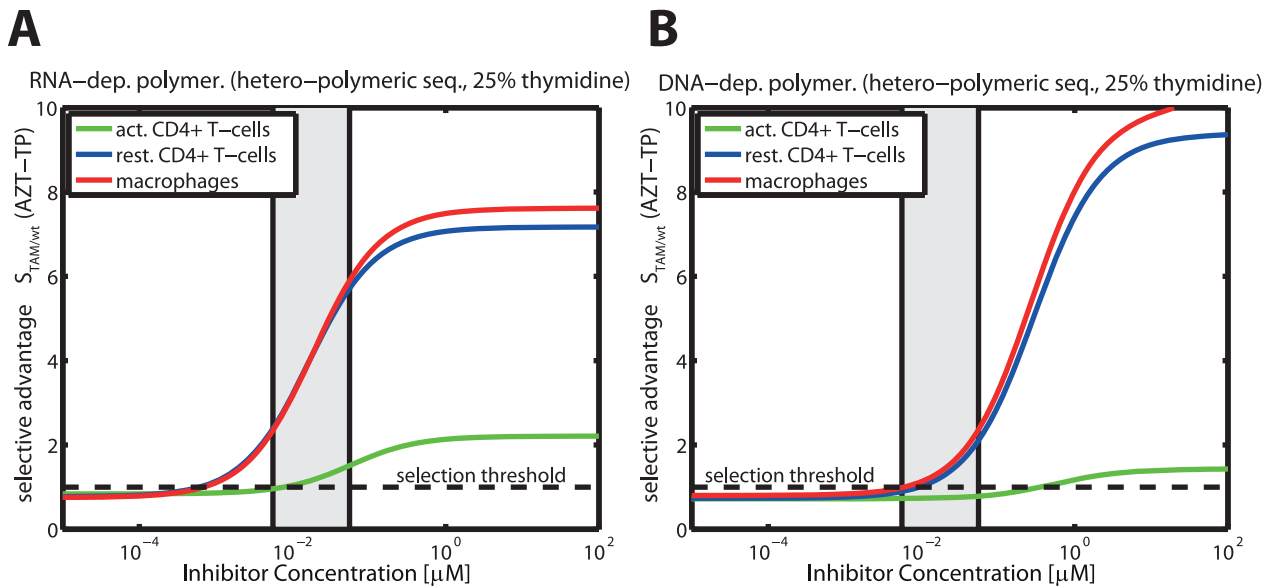


Figure 6. Selective advantage of the 'D67N/K70R/T215Y/K219Q' mutant against the wild type during RNA- and DNA-dependent polymerization in the presence of AZT-TP. The solid lines (green = activated CD4⁺ cells, blue = unstimulated CD4⁺ cells, red = macrophages) indicate the selection parameter $S_{TAM/wt}(AZT-TP)$, defined in eq. (4), for different levels of intracellular AZT-TP during RNA- and DNA dependent polymerization (Panels A & B) of a random sequence of length 500 with 25% respective dNTP content. The light grey area indicates the *in vivo* concentrations range of AZT in purified circulating CD4⁺ T-cells from [71], converted to units μM by assuming a cell volume of $180 \mu m^3$ for resting CD4⁺ T-cells [72]. The dashed horizontal line indicates the threshold for resistance selection, i.e. $S = 1$. All utilized parameters are indicated in Table 1 and Tables S1, S2, S3 (supplementary material). doi:10.1371/journal.pcbi.1002359.g006

Two major findings can be derived from Fig. 6: Firstly, it can be seen that in the case of RNA-dependent polymerization, the 'D67N/K70R/T215Y/K219Q' mutation becomes selected ($S_{TAM/wt}(AZT-TP) \geq 1$; dashed horizontal black line) at lower intracellular AZT-TP concentrations (below clinically achieved concentrations in resting CD4⁺ T-cells and macrophages; light grey area) compared to DNA-dependent polymerization. During DNA-dependent polymerization, 'D67N/K70R/T215Y/K219Q' is only selected at clinically relevant levels of AZT-TP (resting CD4⁺ T-cells and macrophages) or far above (activated CD4⁺ T-cells). We have shown previously in Fig. 4C & D that inhibition of RNA-dependent polymerization by AZT-TP is much more efficient compared with inhibition of DNA-dependent polymerization (see also Table 3), explaining the higher selective pressure exerted at lower AZT-TP concentrations during RNA-dependent polymerization. Therefore, we would expect that resistance is favored at lower concentrations during RNA-dependent polymerization, when compared to DNA-dependent polymerization.

Secondly, and quite surprisingly, Fig. 6A & B indicate that resistance to AZT may not become selected over the wildtype in activated CD4⁺ cells as it only confers a very small selective advantage in these cell types during RNA-dependent polymerization and at clinically relevant concentrations of AZT-TP (solid green line and grey area in Fig. 6A). For DNA-dependent polymerization the selection parameter indicates a disadvantage ($S_{TAM/wt}(AZT-TP) < 1$) of the 'D67N/K70R/T215Y/K219Q' mutant at clinically relevant AZT-TP concentrations. In resting CD4⁺ T-cells and macrophages on the other hand, resistance selection is favored at clinically relevant AZT-TP concentrations (DNA-dependent polymerization) and below (RNA-dependent polymerization). These results indicate, that selection of the 'D67N/K70R/T215Y/K219Q' mutation by AZT is cell-specific and may preferably occur within resting CD4⁺ T-cells and macrophages, whereas resistance selection in activated CD4⁺ T-

cells is less likely. This finding, however, warrants further investigation of the intermediate strains in the TAM resistance pathway, once kinetic data becomes available.

Subsequent selection of Q151M-complex mutations by TDF. The selective advantages of intermediate viral strains of the Q151M-complex (multi-drug) resistance pathway (Q151M, A62V/V75I/F77L/F116Y/Q151M (Q151Mc) and Q151Mc/K70Q) with respect to increasing tenofovir diphosphate (TFV-DP) concentrations are shown in Fig. 7 for DNA-dependent polymerization in resting CD4⁺ T-cells. Panel A shows the selective advantage of the respective mutant in relation to the wild type, i.e. $S_{Q151M/wt}(TFV-DP)$ (dashed blue line), $S_{Q151Mc/wt}(TFV-DP)$ (solid green line) and $S_{Q151Mc+K70Q/wt}(TFV-DP)$ (dotted magenta line). At *in vivo* concentrations ranges of TFV-DP (light grey area) the selective pressure towards the Q151M and the Q151Mc strains is relatively weak ($1 < S_{Q151M/wt}(TFV-DP) \leq S_{Q151Mc/wt}(TFV-DP) < 3$), whereas it is strong for the Q151Mc/K70Q mutant ($4 < S_{Q151Mc+K70Q/wt}(TFV-DP) < 10$). It can be seen that the selective advantage is of the order $S_{Q151M/wt}(TFV-DP) \leq S_{Q151Mc/wt}(TFV-DP) < S_{Q151Mc+K70Q/wt}(TFV-DP)$, indicating a distinctly graded 'selection landscape' from the wild type towards the Q151Mc/K70Q mutant. A graded landscape would imply that the presence of TFV-DP favors subsequent resistance mutations in the resistance pathway. We therefore further analyzed the form of the 'selection landscape' in panel B, where we have plotted the selective advantage of the respective mutants in relation to their progenitors in the resistance pathway, i.e. $S_{Q151M/wt}(TFV-DP)$, $S_{Q151Mc/Q151M}(TFV-DP)$, $S_{Q151Mc+K70Q/Q151Mc}(TFV-DP)$. It can be seen that the Q151M single mutation has a weak selective advantage over the wild type ($S \approx 2$ dashed blue line). The Q151M-complex (Q151Mc) has an even weaker selective advantage over the Q151M single mutation in the presence TFV-DP ($S < 1.5$, solid green line). However, the subsequent mutation, Q151Mc → Q151Mc/K70Q has a strong

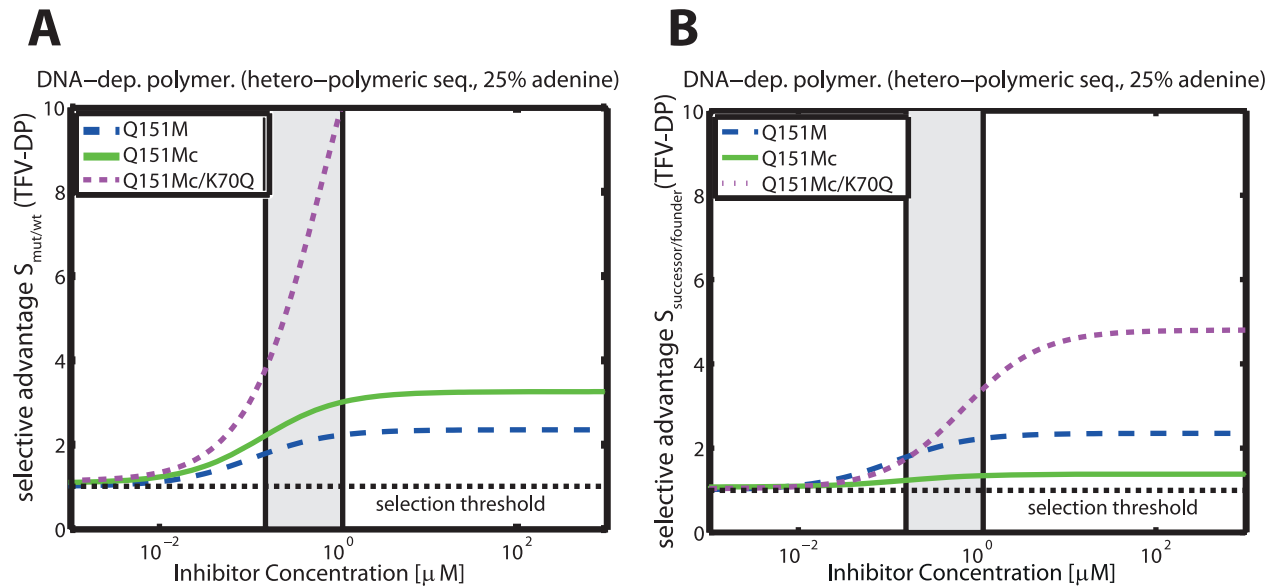


Figure 7. Selective advantage S of intermediate viral mutants of the Q151M-complex during DNA-dependent polymerization in the presence of TFV-DP. Dashed blue-, solid green- and dotted magenta line indicate the selective advantage of the Q151M, the multi-drug resistant Q151M-complex (Q151Mc: A62V/V75I/F77L/F116Y/Q151M) and the Q151Mc+K70Q mutation during DNA-dependent polymerization of a random sequence of length 500 with 25% respective dNTP content in unstimulated CD4⁺ cells. The light grey area indicates the *in vivo* concentrations range of TFV-DP from [56,71,73], converted to units μM by assuming a cell volume of $180\mu\text{m}^3$ for resting CD4⁺ T-cells [72]. The dashed horizontal line indicates the threshold for resistance selection, i.e. $S=1$. Panel A: Selective advantage of the respective mutants with regard to wild type $S_{\text{mut}/\text{wt}}$ (TFV-DP). B: Selective advantage of a succeeding mutants with regard to progenitor in Q151M complex formation $S_{\text{mut1}/\text{mut2}}$ (TFV-DP). All utilized parameters are indicated in Table 1 and Tables S1, S2 (supplementary material). doi:10.1371/journal.pcbi.1002359.g007

selective advantage in the presence of TFV-DP ($S > 2$). The selection landscape therefore exhibits a slight increase (wt \rightarrow Q151M), followed by a plateau (Q151M \rightarrow Q151Mc), followed by a steep increase (Q151Mc \rightarrow Q151Mc/K70Q). Our analysis indicates that TDF treatment slightly favors Q151M over the wild type, it, however, does not favor the Q151M-complex $S_{\text{Q151Mc}/\text{Q151M}}$ (TFV-DP) ≈ 1 . Once the Q151M-complex has arisen (due to co-administered drugs), TDF could select for the K70Q mutation.

Epistasis

Epistasis has been used to describe the phenomenon where the phenotype of one mutation is modified by one or several other mutations [22,23]. In a two-locus-two allele model, epistasis is said to be positive when the combined effects of a double mutant result in greater replication than expected if the effects on replication coming from the two single mutations were independent. Conversely, epistasis is said to be negative, when the combined effects of a double mutant result in lesser than expected replication. Resistance mutations against NRTIs of HIV-1 are located within the same gene (the *Pol* gene). It is therefore likely, that the combination of mutations produce a phenotype that has unexpected/novel properties. The intention of this analysis is to elucidate how epistasis depends on the environment in which the virus replicates (and which is altered by NAs), analogously to [23]. In Fig. 8, we assessed epistasis with regard to replication (solid blue line), fitness (solid red line) and resistance (solid green line), based on eqs. (5)–(7) for the K65R/M184V mutant and varying TFV-DP concentrations for DNA-dependent polymerization in resting CD4⁺ T-cells.

It can be seen that epistasis in the absence of drugs $E_f(\phi)$ (fitness epistasis) is positive (solid red line). This result is based on the fact

that the predicted fitness of the double mutant $f_{\text{M184V}/\text{K65R}} = 30\%$ is larger than expected if the fitness effects coming from the respective single mutants $f_{\text{M184V}} = 46\%$ and $f_{\text{K65R}} = 38\%$ were independent. Resistance epistasis $E_{\text{Res.}}(\text{NA})$ (green line) on the other hand is negative at clinically relevant TFV-DP concentrations (light grey area). Whereas the M184V mutation is slightly hypersusceptible (predicted fold resistance relative to the wild type: 0.76 see also [40]), the K65R mutation confers ≈ 5.3 -fold resistance in relation to the wild type, mainly by decreasing TFV-DP's incorporation rate k_{term} , see Table S2 (supplementary information). We predicted that the double mutant 'M184V/K65R' is ≈ 2 -fold resistant in relation to the wildtype. Resistance epistasis $E_{\text{Res.}}(\text{NA})$ thus reduces replication of the double mutant in the presence of TFV-DP and is negative. The combined effects of fitness and drug resistance are indicated by the blue line in Fig. 8. Our predictions indicate that epistasis is positive at clinically relevant TFV-DP concentrations (light grey area), because the (positive) fitness epistasis outweighs the negative resistance epistasis in the clinically relevant range of TFV-DP concentrations. At higher TFV-DP concentrations, however, the negative resistance epistasis outweighs.

Residual DNA-dependent polymerization of mutant reverse transcriptase (RT) of HIV-1 in the presence of distinct nucleoside reverse transcriptase inhibitors (NRTIs)

Viral fitness is an important determinant for the pre-treatment abundance of drug resistant mutants and their persistence in circulating virus after withdrawal of drugs. Moreover, it has also important implications for the therapeutic strategy and on disease progression [20,21]. For these reasons, we assessed viral fitness of the distinct mutants in the absence of drugs. We estimated viral

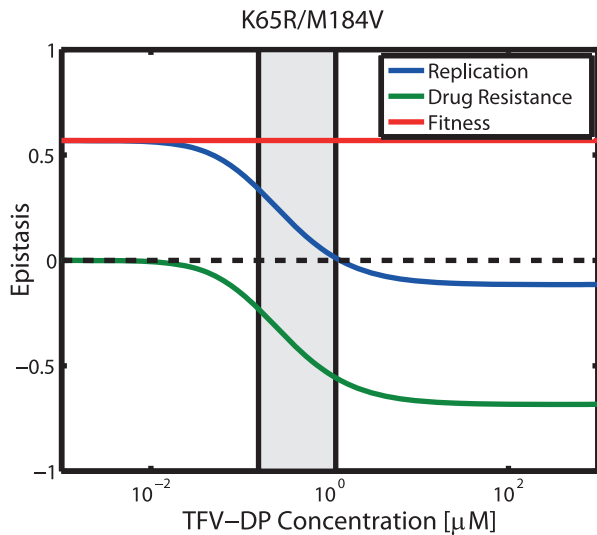


Figure 8. Epistatic interactions for DNA-dependent polymerization in the presence of TFV-DP. Solid blue-, green- and red line indicate epistasis with regard to replication $E_{\text{Rep.}}(\text{NA})$, resistance $E_{\text{Res.}}(\text{NA})$ and fitness $E_f(\phi)$ as defined in eqs. (5)–(7) for the double mutant ‘K65R/M184V’. The black dashed horizontal line indicates the value, where no epistatic interactions occur. The light grey area indicates the *in vivo* concentrations range of TFV-DP from [56,71,73], converted to units μM by assuming a cell volume of $180\mu\text{m}^3$ for unstimulated CD4^+ T-cells [72]. All utilized parameters are indicated in Table 1 and Tables S1, S2 (supplementary material). doi:10.1371/journal.pcbi.1002359.g008

fitness on the basis of the relative decrease in polymerization time, see eq. (3), for a hetero-polymeric sequence context and based on DNA-dependent polymerization during reverse transcription. The results are presented in Table 4 (bottom row). The fitness of the viral mutants was of the order $\text{K65R/M184V} < \text{K65R} \leq \text{M184V} < \text{Q151M} \approx \text{wildtype}$ and is in general agreement with published data on viral fitness [21,41]. Notably, the K65R and M184V mutants conferred substantial fitness losses, which explains the low prevalence of K65R even in treatment experienced patients [21], and M184V reversion to wild type when 3TC, ABC or FTC are eliminated from second or third-line anti-retroviral regimens [42].

Estimated residual DNA-dependent polymerization for mutant and wild type RT under *in vivo* concentration ranges of triphosphorylated NRTIs in resting CD4^+ T-cells and on a hetero-polymeric sequence context (using eqs. (1)–(2)) are presented in Table 4. Utilized kinetic parameters for nucleoside incorporation are provided in Table S2 (supplementary material). We predicted that most inhibitors decreased DNA-dependent polymerization to values of 2–25% in the wildtype enzyme. However, 3TC displayed superior efficacy (only 1.5–5% residual polymerization) and AZT only poorly inhibited DNA-dependent polymerization. However, as discussed in section *Residual polymerization in the presence of AZT*, AZT is likely to exert its main effect through inhibition of RNA-dependent polymerization. The Q151M mutation decreased the efficacy of carbovir triphosphate (CBV-TP) markedly (8 fold) and had only marginal impact on tenofovir diphosphate (TFV-DP), whereas lamivudine triphosphate (3TC-TP) and emtricitabine triphosphate (FTC-TP) were unaffected (see also [40,43]). Combination treatment with 3TC-TP+CBV-TP could, however, restore inhibition of polymerization and combination treatment FTC-TP+TFV-DP was very efficient, however not markedly

Table 4. Estimated *in vivo* % residual DNA-dependent polymerization ($1 - \epsilon$) for distinct mutants and drug combinations.

	wt	Q151M	M184V	K65R	M184V/ K65R
TFV-DP	4.16–24.11	9.20–42.55	3.32–20.05	19.11–63.34	8.72–41.14
AZT-TP	29.47–80.69	-	-	-	-
d4T-TP	2.08–25.95	-	7.44–56.97	-	-
FTC-TP	2.07–21.45	1.24–14.00	-	21.28–77.76	47.37–92.09
3TC-TP	1.54–4.95	0.86–2.81	51.22–77.71	12.29–31.77	86.19–95.40
CBV-TP	7.63–14.18	82.27–90.27	45.49–62.53	-	-
FTC-TP	1.39–12.69	1.11–11.75	-	11.02–53.12	7.80–39.22
+TFV-DP					
d4T-TP	0.91–4.40	-	7.01–49.20	-	-
+3TC-TP					
CBV-TP	1.33–3.89	0.87–2.84	32.20–53.53	-	-
+3TC-TP					
CBV-TP	1.27–3.81	-	-	-	-
+3TC-TP					
+AZT-TP					
fitness	100	100	46	38	30

In vivo concentration ranges were 3TC-TP = 12.2–40.5; FTC-TP = 1.5–19.4; TFV-DP = 0.16–1.17; CBV-TP = 0.44–0.88; d4T-TP = 0.034–0.56; and AZT-TP = 0.0056–0.056 μM respectively [56,71,73–75], assuming an average cell volume of $180\mu\text{m}^3$ for resting CD4^+ T-cells [72]. doi:10.1371/journal.pcbi.1002359.t004

different from FTC-TP alone. The M184V mutation decreased susceptibility to 3TC-TP (≈ 20 fold) and CBV-TP (8 fold), having marginal impact on stavudine triphosphate (d4T-TP) and no effect on TFV-DP, which is consistent with phenotypic measurements [40,43]. Susceptibility to the combination of d4T-TP+3TC-TP was comparable to d4T-TP alone. The efficacy of 3TC-TP+CBV-TP was strongly reduced. We predicted that the K65R mutation reduced the impact of 3TC-TP, FTC-TP and TFV-DP (7-, 4 and 3-fold respectively) and also reduced the susceptibility to the combination FTC-TP+TFV-DP (5-fold), consistent with phenotypic measurements [40,43]. The double mutation K65R/M184V conferred complete resistance to 3TC-TP and near complete resistance to FTC-TP and partly restored susceptibility to TFV-DP or TFV-DP+FTC-TP, compared to K65R alone, in agreement with phenotypic measurements [40,43].

Inhibition of human mitochondrial polymerase γ by various NRTIs

Despite their antiviral activity, NRTIs have been reported to cause severe mitochondrial toxicity [9,44], limiting their therapeutic use. A dominant hypothesis for the manifestation of mitochondrial toxicity by NRTIs is that NRTIs inhibit polymerase- γ ($\text{pol}-\gamma$) function, which is necessary to duplicate the mitochondrial genome, thereby leading to mtDNA depletion and subsequent mitochondrial abnormalities. The anticipated mechanism of $\text{pol}-\gamma$ inhibition is highly similar to inhibition of polymerization during reverse transcription: tri-phosphorylated NRTIs compete with endogenous dNTPs for incorporation into the nascent mtDNA, and, once incorporated, lead to quasi-chain

termination [9]. Polymerase- γ can perform two crucial catalytic functions, namely DNA polymerization and exonuclease activity; the later enabling the removal of incorporated NRTIs. The mechanism of action of NRTIs on pol- γ leads us to believe that our mathematical model of polymerase inhibition by **NAs** can be useful in predicting NRTI-induced inhibition of pol- γ .

Utilizing pre-steady state kinetic data for the incorporation of dNTPs and various NRTIs (see Table S4, supplementary material), we estimated the residual pol- γ function in a hetero-polymeric sequence context and under concentration ranges of NRTI-TPs typically observed *in vivo*. The results are stated in Table 5. For simulation purposes we utilized eqs. (1) and assumed dNTP levels typically observed in unstimulated CD4⁺ cells (see Table 1). Under the parameters used, we found that mtDNA polymerization is substantially inhibited in the presence of d4T-TP and moderately inhibited by 3TC-TP for *in vivo* -triphosphate concentration ranges. Similarly, combinations 3TC-TP+d4T-TP reduced pol- γ activity substantially and 3TC-TP+CBV-TP or 3TC-TP+AZT-TP+CBV-TP reduced pol- γ activity moderately. We found the following order of inhibition of polymerase- γ : d4T-TP > 3TC-TP > TFV-DP \geq FTC-TP \geq AZT-TP \geq CBV-TP, which agrees with experimental findings [9]. The mitochondrial toxicity of AZT is likely not due to pol- γ inhibition. Instead, it has been explained in terms of various other mechanisms, which are exemplified in the Discussion section.

We subsequently defined a therapeutic index as the ratio of the mean inhibition of pol- γ and wild type RT respectively. The therapeutic index indicated the following order for the inhibitors and their combinations: d4T-TP < d4T-TP + 3TC-TP < TFV-DP < FTC-TP \leq CBV-TP < FTC-TP + TFV-DP < 3TC-TP < CBV-TP + 3TC-TP. Note, that AZT has been excluded from this assessment, because its mitochondrial toxicity has been contributed to mechanisms other than pol- γ inhibition (see Discussion section).

Discussion

We presented a novel mechanistic mathematical model of HIV-1 polymerase inhibition by **NAs** that, for the first time, focussed on the transient aspect of this inhibition. This is an important characteristic, as HIV-1 can exploit the transient nature of inhibition by reducing the residence time of the apparent chain terminator (the incorporated **NA**) in the nascent viral DNA to achieve drug resistance (summarized in [13]). **NA** removal from quasi-terminated RNA/DNA chains has also been described for hepatitis B & C viruses [24–26]. Hence, the developed model may also be applicable to study polymerase inhibition by **NAs** in these viruses. In contrast to previous mathematical approaches [14,19], we therefore describe the effects of nucleoside analogs on DNA-polymerization in terms of an increase in the average polymerization time, which is analogous to a reduction of the overall polymerization rate, i.e. $\bar{v}_{poly}(\phi) = 1/T_{0 \rightarrow N}(\phi)$. This mathematical approach not only allows to study various resistance mechanisms, but also allows for the first time to estimate the inherent fitness of drug resistant mutants, resulting from microscopic changes in the polymerization rate constants (e.g. k_{pol} , $K_{D,dNTP}$) of the mutant viral enzyme (see eqs. (1)–(3)). The derived model can readily be used to assess the probability to successfully finish polymerization. In supplementary Text S1 we have given an example for HIV-1 reverse transcription. It is also explained therein how the model can be integrated in larger (systems biology) models of the viral life cycle in order to study the effects of **NAs**.

The developed model can be parameterized in terms of physiological parameters (such as dNTP concentrations) and microscopic kinetic rates (e.g. k_{pol} , k_{term} , K_D), typically derived from cell-free *in vitro* assays. These parameters can usually be precisely determined with standard errors <20%. We demonstrated the applicability of the model for various distinct polymerization processes, in particular for polymerase inhibition during HIV-1 RT and mitochondrial pol- γ by NRTIs, respectively. Adaptation to distinct polymerization processes was achieved by utilizing the kinetic constants for the respective processes, while the model remained unchanged. Notably, model-predicted macroscopic predictions (viral fitness, drug efficacy and toxicity) were consistent with various experimental macroscopic findings and thus underline the usefulness of the proposed model.

Based on the developed model of polymerization and its inhibition by **NAs**, we derived two sets of mathematical solutions: Eqs. (1)–(11) can be used to compute the average effect of **NAs** and combinations of **NAs** on polymerization of arbitrary (hetero-polymeric) DNA sequences. Analogously, these equations can be used to determine the deceleration of polymerization resulting from resistance mutations in the absence of any **NA**, as an indicator of their inherent fitness cost. On the other hand, eqs. (16)–(20) represent analytical solutions for polymerase inhibition by **NAs** in a simplified homo-polymeric sequence context. The resulting equations (19)–(20) immediately highlight key determinants of **NA** inhibition and resistance development in this context. These equations can also be used to determine the model's sensitivity for different combinations of kinetic- and physiological parameters, see Fig. 3 and Fig. 5. Based on eqs. (19)–(20), we found that factors impacting on **NA** inhibition can generally be divided into two categories: (i) kinetic- and (ii) cellular factors.

Eq. (20) revealed that the rate of **NA** incorporation k_{term} , its binding affinity $K_{D,NA}$ and the catalytic rate of **NA** removal r_{exc} are key molecular kinetic determinants for the efficacy of **NAs**. All indicated molecular kinetic determinants (k_{term} , $K_{D,NA}$ and r_{exc}) depend on the viral polymerase enzyme and are thus prone to resistance development. The impact of alterations in these

Table 5. Estimated *in vivo* % residual human mitochondrial polymerase- γ activity in resting CD4⁺ cells.

	(1 - ϵ_{tox})	ther. Index*
TFV-DP	63.54–92.72%	5.5
AZT-TP	98.74–99.87%	†
d4T-TP	0.15–2.40%	0.1
FTC-TP	94.05–99.51%	8.2
3TC-TP	25.69–53.43%	12.2
CBV-TP	98.78–99.38%	9.1
FTC-TP/TFV-DP	61.96–92.55%	11
3TC-TP/d4T-TP	0.16–2.48%	0.5
CBV-TP/3TC-TP	25.18–52.70	14.9
CBV-TP/3TC-TP/AZT-TP	26.22–54.13%	†

In vivo concentration ranges were 3TC-TP = 12.2–40.5; FTC-TP = 1.5–19.4; TFV-DP = 0.16–1.17; CBV-TP = 0.44–0.88; d4T-TP = 0.034–0.56; and AZT-TP = 0.0056–0.056 μ M, respectively [56,71,73–75], assuming an average cell volume of 180 μ m³ for resting CD4⁺ T-cells [72].

*calculated as the ratio of average effect on polymerase- γ and wildtype reverse transcriptase of HIV-1: $(1 - \epsilon_{tox}) / (1 - \epsilon_{RT-wt})$.

†mitochondrial toxicity of AZT has been attributed to mechanisms other than pol- γ inhibition (see Discussion section).

doi:10.1371/journal.pcbi.1002359.t005

parameters is illustrated in Fig. 3B for ddATP and in Fig. 4 & 5 for AZT-TP.

Various reports indicate cell-specific differences in NA efficacy against HIV-1 [45–47]. Differences in efficacy were often brought in association with intracellular NA-TP:dNTP ratios [48,49]. Utilizing the derived model, we elucidated the impact of cellular factors on HIV-1 RT polymerase inhibition by NRTIs. Quite surprisingly, we found that cells that contain low dNTP content do not necessarily confer hypersusceptibility to NRTIs if $[dNTP] \ll K_{D,dNTP}$ (see Fig 3A). For AZT, we predicted that alteration of PPI and ATP levels can have a strong impact on its efficacy (see Table 3). In summary, we demonstrated that the concurrence of multiple kinetic- and physiological factors, rather than a single parameter, can determine the susceptibility of an infected cell towards NAs, see eq. (20)–(21). In addition to cells that contain an unfavorable NA-TP:dNTP ratio [48,49], cells that contain high levels of PPI or ATP and low levels of NA (regardless of their dNTP content) could be resistant to NRTI treatment and residual viral replication despite treatment could persist in these cells as well. This finding can have important consequences for HIV-1 treatment with NRTIs, as HIV-1 exhibits a broad cell tropism [28–32]: While some evidence for low-level ongoing replication in the context of apparently suppressive antiviral therapy has been reported [50], the cellular source remains to be determined [51]. Whereas it has been shown previously [33], that heterogeneous viral inhibition facilitates drug resistance development, we show evidence for cell-specific (thus heterogeneous) inhibition by NRTIs. Thus, a possible mechanism for the emergence of drug resistance against could be explained on the basis of the mechanism of action of these compounds. However, further evidence is required to confirm this hypothesis.

We analyzed the specific mechanisms of AZT resistance through TAMs. It is well known, that TAMs induce resistance through increasing the excision of incorporated NAs from nascent viral DNA. However, the precise mechanism that increases excision is controversial. A recent crystal structure of resistant RT [39], showed that the orientation of ATP is altered in the mutant enzyme. Based on this structure [39], the authors argued that ATP, which serves as an excision substrate for incorporated AZT, would bind with higher affinity to the quasi-terminated nascent viral DNA, accelerating the removal of incorporated AZT. To the contrary, our kinetic model indicated that increasing the affinity for ATP binding $K_{D,ATP}$ does not lead to resistance development (see Fig. 5), because ATP binding to the wild type enzyme is already saturated ($K_{D,ATP} < [ATP]$) at physiological conditions, and further decrease of $K_{D,ATP}$ enhances the saturation effect. Increasing the removal rate k_{ATP} desensitizes reverse transcriptase-mediated polymerization to AZT inhibition since $r_{exc} \approx k_{ATP}$, in cells with low PPI contents and under saturation conditions (see Table 1 and eq. (21)). We therefore propose that the main kinetic resistance effect of the altered orientation of ATP in mutant RT is mediated by an increased removal rate k_{ATP} , in agreement with a pre-steady state kinetic analysis [17], although binding could be affected. In particular, the crystal structure showed that the resistance mutations affect the positioning of ATP in the RT catalytic site [39], which must translate into an effect on k_{ATP} .

We quantified the inhibitory effects of AZT during RNA- and DNA dependent polymerization and we analyzed how TAMs ('D67N/K70R/T215Y/K219Q') induce susceptibility changes. We found that AZT inhibition during HIV-1 reverse transcription is more efficient during RNA-dependent polymerization than during DNA-dependent polymerization, see Fig. 4. Moreover,

inhibition, as well as susceptibility changes induced by TAMs were found to be cell-specific (see Table 3).

While the emergence of a particular viral strains depends on a) the probability that the mutant is generated (related to residual replication and genetic distance), it also critically depends on the likelihood that the generated mutant becomes selected subsequently. However, if inhibition- and selection forces are different in distinct target cells (see Table 3 and Fig. 6), then the processes of mutant strain generation and subsequent selection might also be divided among target cells. We therefore further looked at the selective advantage $S_{TAM/wt}$ of the 'D67N/K70R/T215Y/K219Q' mutant in distinct cell types. Specifically, we predicted that the selective advantage of the 'D67N/K70R/T215Y/K219Q' mutation in the presence of AZT at clinically relevant concentrations is quite distinct in activated $CD4^+$ cells, resting $CD4^+$ cells and macrophages (see Fig. 6). We found that the 'D67N/K70R/T215Y/K219Q' mutation is less likely selected over the wild type in activated $CD4^+$ cells, whereas this mutation is preferred in resting $CD4^+$ cells and macrophages (see Fig. 6) at clinically relevant concentrations. While these results indicate, for the first time, that selection forces against NA treatment can be quite distinct for diverse target cells, a detailed analysis of the various intermediate mutants in the TAM resistance pathway is required, in particular a construction of the 'selection landscape' for particular mutants in the resistance pathway and for different cell types infected with HIV-1 in the presence of combinations of drugs to fully understand resistance dynamics *in vivo*. The developed model can be used to facilitate such an analysis: In Fig. 7, we started to reconstruction the 'selection landscape' for intermediate mutants of the Q151M-complex during TDF treatment in unstimulated $CD4^+$ cells. We found for this cell type, that TDF alone is unlikely to select the Q151M-complex over the Q151M single mutation. Once the Q151M-complex has arisen, however, TDF would select for the additional K70Q mutation. An extended analysis of the resistance pathways in the case where particularly large genetic barriers are involved may in the future help to understand and influence the dynamics of resistance emergence for e.g. TAMs and the Q151M complex.

Epistasis has been suggested as a method to study evolutionary dynamics of virus populations [52]. It describes the phenomenon where the replicative fitness of one mutation is modified by one or several other mutations [22,23]. Epistasis is said to be positive when the combined effects of two-or-more mutations result in greater replication than expected if the effects coming from the two single mutations were independent. Since resistance mutations against NRTIs of HIV-1 are located within the same enzyme (RT), several mutations could modify the enzyme in unexpected ways, i.e. result in epistatic interactions with regard to fitness and resistance. We have shown in Fig. 8 that our model can be used to analyze different aspects of epistasis (fitness, resistance and replication). In the presented example, we detected positive fitness epistasis E_f of the 'M184V/K65R' double mutant and negative resistance epistasis $E_{Res}(NA)$ with increasing TFV-DP concentrations in comparison with the single mutations. The combined effects of fitness- and resistance were positive at relevant concentration ranges of TFV-DP. The major conclusion from this analysis is that the combination of mutations can alter the RT enzyme in unexpected ways. The phenotypic attributes of a multiple mutated strain may not be intuitively related to the attributes of the single mutants. It is thus required to view each multiple mutated strain as an independent entity with regard to resistance and fitness. For deriving information about intermediate viral mutants in a resistance pathway (e.g. the Q151M-complex, or TAMs), it is therefore necessary to measure the attributes of each

intermediate strain independently. Related experimental work [23] indicated that replication ranking, rather than epistasis predicts dynamics of resistance emergence, in line with our analysis in section “*Selection of Resistance*”.

Based on the developed model, we predicted that the ‘D67N/K70R/T215Y/K219Q’ mutation induces a 4.1 to 22.6 fold increase in the IC_{50} value for poly-thymidine polymerization, depending on the cell type and the template (RNA or DNA). In cellular assays, the ‘D67N/K70R/T215Y/K219Q’ mutant can induce a 120–150 fold increase in the fifty percent inhibitory (extracellular) concentration when measured in $CD4^+$ HeLa-cells [46] and a 8000 fold increase in MT-4 human T-lymphoid cells [47], respectively, while at the same time resistance at the enzymatic level was observed to be far more moderate [47]. This indicates that a direct quantitative comparison of susceptibility changes observed in different cell-based assays and changes computed at the enzymatic level, e.g. on the basis of DNA-dependent polymerization in resting $CD4^+$ cells (see Table 3) might not be possible. Here, we summarize a few mechanisms, which could contribute to this difference: (i) Firstly, the cell types utilized in distinct cell-based assays differ, which can result in distinct susceptibility changes to NRTIs. We discussed- and illustrated the impact of these cell-specific differences in *Cell type specific susceptibility to AZT and impact of resistance* and in Table 3 for AZT. For AZT, these cell-specific differences were attributed to different contents of PPi and dTTP. (ii) Secondly, two different outputs are measured by the two methods: In contrast to RT activity, phenotypic assays measure the production of viral proteins, which denotes a step in the viral life cycle following polymerization and reverse transcription of the viral genome. (iii) Thirdly, and most importantly, the IC_{50} values based on enzymatic activity (as computed in this work) refer to intracellular concentrations of AZT-triphosphate, while the fold change derived by cell-based assays refers to the concentrations of extracellular pro-drug (AZT) added to the medium surrounding the cells. This has important consequences: AZT phosphorylation is known to be non-linear and might be saturated at the bottleneck step of thymidilate kinase (monophosphate \rightarrow diphosphate) [53,54]. We have shown previously that the *in vivo* maximally achievable AZT-TP concentration is close to the clinically achieved AZT-TP concentration in peripheral blood mononuclear cells (PBMCs), when 300 mg AZT is given twice daily, see [53]. In order to disproportionately increase the IC_{50} (AZT) value several hundred-fold, as observed with some mutants e.g. ‘M41L/D67N/K70R/T210W/Y215F’, at the enzymatic level all that is required is a minor fold change in the IC_{50} (for AZT-TP), that shifts the fifty percent inhibitory concentration of intracellular AZT-TP beyond the maximally achievable levels. Thus, by adding more extracellular AZT, sufficient concentrations of AZT-TP may never be reached. In the case of saturating intracellular AZT monophosphate (AZT-MP) concentrations, the cell-specific levels of thymidilate kinase enzyme will ultimately determine the maximally achievable AZT-TP concentration, which are therefore also cell-specific [55].

In Table 4 we analyzed, based on the developed model, how different mutations can specifically alter the efficacy of distinct NRTIs and their combinations on DNA-directed polymerization and at physiological concentrations. Estimated susceptibility changes resulting from distinct mutations were *qualitatively* in good agreement with results from cell culture assays (see [40]), although, as mentioned earlier, it should be noted that a direct *quantitative* comparison of our estimations with results from cell-culture assays may not be possible. While estimating the effect of combinations of NAs on DNA polymerization is straightforward using eq. (1)–(11),

we did not assess clinically relevant pharmacokinetic interactions between different NAs. Pharmacokinetic interactions between NRTIs of HIV-1 have mainly been attributed to interactions during the cellular activation cascade [56]. For our estimations in Table 4 we therefore assessed only drug combinations that use distinct enzymes in their phosphorylation cascade and which therefore bear lesser potential for pharmacokinetic interaction than drugs which utilize the same intracellular phosphorylation pathway.

Inhibition of mitochondrial polymerase- γ by NRTIs has been proposed as a central process for their clinical toxicity [9]. We therefore studied inhibition of polymerase- γ by distinct NRTIs at physiologically relevant triphosphate concentrations. The ranking of polymerase- γ inhibition by the analyzed NRTIs was in good agreement with published results [9], indicating a strong inhibition of pol- γ by d4T and moderate inhibition by 3TC at physiological intracellular triphosphate concentrations. However, it should also be noted, that mitochondria in different tissues might contain different levels of dNTP and NRTI-TPs and might therefore be differentially prone to pol- γ inhibition, potentially contributing to site-specific toxicities of some NRTIs [9]. Mitochondrial toxicity of AZT has been explained by other mechanisms than pol- γ inhibition. In particular, AZT might deplete dNTP pools in the mitochondria, rather than quasi-terminate nascent mtDNA by its incorporation [57,58].

Although we demonstrated the use of the developed model on nucleoside reverse transcriptase inhibitors of HIV-1 throughout the article, we did not construct a mathematical model of the complete reverse transcription process, but rather focussed on the sub-process of polymerization, which is primarily targeted by NRTIs and other NAs. The aim was to point out general principles of inhibition and resistance development, rather than establishing customized models for the respective targeted viral processes. Therefore, the presented model can be used to also assess effects on distinct polymerase enzymes, or as demonstrated in Table 5 to assess off-target effects of NAs. Furthermore, the model can readily be used to assess inhibition of polymerization by NcRTIs, a novel class of pre-marketed nucleoside inhibitors which compete with natural dNTPs for binding to the polymerase enzyme, without becoming incorporated [59–61].

In the future, the developed model could be extended for the “dead-end complex”-mechanism observed during inhibition of HIV-1 RT [13], if respective kinetic parameters become available. Extension of the model is straightforward, as it only requires the introduction of an additional state in the mathematical model ($\tilde{I} \rightleftharpoons \dagger$ in Fig. 1) and the subsequent derivation of the corresponding equations, analogously to the derivations in this article.

Recent *in vitro* experiments with single-molecules of HIV-1 RT indicated that additional complexities might occur during the reverse transcription process, such as enzyme-template dissociation and association and reversal of orientation to perform distinct tasks, such as RNase H cleavage of the viral RNA template [62,63]. While these results warrant further investigation, it has been shown that *in vivo* an excess of RT (50–200 enzymes/virion) in comparison to RNA template may be present [64], such that different enzymes could perform different tasks (polymerization/RNase H) at the same time *in vivo*. The cooperativity of multiple RT enzymes can also explain the distinct shape of the dose-response curve observed in primary human cells with inhibitors that directly target the enzyme, such as non-nucleoside reverse transcriptase inhibitors (NNRTIs), in contrast to inhibitors that target the RNA/DNA template (NRTIs) [65,66]. The development of models of reverse transcription that also incorporate the effects of non-nucleoside reverse transcriptase inhibitors (NNRTIs) [67,68] warrants further mechanistic understanding of the

complex overall process of reverse transcription and will be left for future research. The developed model can however be readily be used to model the effects of NAs and will be further extended to model e.g. the complete reverse transcription process of HIV-1 genomic RNA, or analogous processes in other viruses (see also supplementary Text S1).

Methods

Derivation of a recursive solution for the polymerization times on arbitrary hetero-polymeric sequences

In this section we will derive the analytical solution for the polymerization time given in eq. (10), which is based on ideas given in [69]. Recall that the proposed model is a Markov jump process and that the polymerization time $T_{0 \rightarrow N}$ is given by the *mean first passage time* (MFPT) to go from state ‘0’ (initiation of polymerization) to the state ‘N’ (final polymerization product).

Starting point for the derivation are the MFPT-equations ($i=0, \dots, N-1$) [70],

$$-1 = -(r_{\text{pol}}(i+1) + r_{\text{pyro}}(i) + r_{\text{term}}(i+1))T_{i \rightarrow N} + r_{\text{pol}}(i+1) \cdot T_{i+1 \rightarrow N} + r_{\text{pyro}}(i) \cdot T_{i-1 \rightarrow N} + r_{\text{term}}(i+1) \cdot T_{i+1 \rightarrow N}^{\sim} \quad (22)$$

$$-1 = -r_{\text{exc}}(i+1) \cdot T_{i+1 \rightarrow N}^{\sim} + r_{\text{exc}}(i+1) \cdot T_{i \rightarrow N}. \quad (23)$$

Eq. (23) yields

$$T_{i+1 \rightarrow N}^{\sim} = \frac{1}{r_{\text{exc}}(i+1)} + T_{i \rightarrow N}$$

such that eq. (22) simplifies to

$$-1 = -T_{i \rightarrow N}(r_{\text{pol}}(i+1) + r_{\text{pyro}}(i) + r_{\text{term}}(i+1)) + r_{\text{pol}}(i+1) \cdot T_{i+1 \rightarrow N} + r_{\text{pyro}}(i) \cdot T_{i-1 \rightarrow N} + \frac{r_{\text{term}}(i+1)}{r_{\text{exc}}(i+1)} + r_{\text{term}}(i+1) \cdot T_{i \rightarrow N}.$$

Further algebraic rearrangements yield

$$-1 = -T_{i \rightarrow N}(r_{\text{pol}}(i+1) + r_{\text{pyro}}(i)) + r_{\text{pol}}(i+1) \cdot T_{i+1 \rightarrow N} + r_{\text{pyro}}(i) \cdot T_{i-1 \rightarrow N} + \frac{r_{\text{term}}(i+1)}{r_{\text{exc}}(i+1)},$$

and finally

$$T_{i \rightarrow N} = \frac{1}{r_{\text{pol}}(i+1) + r_{\text{pyro}}(i)} \left[1 + \frac{r_{\text{term}}(i+1)}{r_{\text{exc}}(i+1)} + r_{\text{pol}}(i+1) \cdot T_{i+1 \rightarrow N} + r_{\text{pyro}}(i) \cdot T_{i-1 \rightarrow N} \right]. \quad (24)$$

We define the general relation

$$T_{i \rightarrow i+1} = T_{i \rightarrow N} - T_{i+1 \rightarrow N}, \quad (25)$$

which allows us to express $T_{0 \rightarrow N}$ as a telescope sum ($T_{N \rightarrow N} = 0$), i.e.,

$$T_{0 \rightarrow N} = \sum_{i=0}^{N-1} T_{i \rightarrow i+1}. \quad (26)$$

From the general relation (25), we can derive $T_{i+1 \rightarrow N} = T_{i \rightarrow N} - T_{i \rightarrow i+1}$ and $T_{i-1 \rightarrow N} = T_{i \rightarrow N} + T_{i-1 \rightarrow i}$, which were substituted into equation (24). Rearrangement produces the recursion

$$T_{i \rightarrow i+1} = \frac{1}{r_{\text{pol}}(i+1)} \left(1 + \frac{r_{\text{term}}(i+1)}{r_{\text{exc}}(i+1)} + r_{\text{pyro}}(i) \cdot T_{i-1 \rightarrow i} \right), \quad (27)$$

which equals

$$T_{i \rightarrow i+1} = (\tau_{i+1}^{\sim} \cdot \rho_{i \rightarrow i+1}^{\sim} + \tau_i + \rho_{i \rightarrow i-1} T_{i-1 \rightarrow i}) \frac{1}{\rho_{i \rightarrow i+1}}, \quad (28)$$

with parameter definitions given in eq. (9) of the main text.

Equation (27) is satisfied by

$$T_{i \rightarrow i+1} = \sum_{k=1}^{i+1} \frac{r_{\text{term}}(k) + r_{\text{exc}}(k)}{r_{\text{pol}}(k) \cdot r_{\text{exc}}(k)} \left(\prod_{j=k}^i \frac{r_{\text{pyro}}(j)}{r_{\text{pol}}(j+1)} \right) \quad (29)$$

such that the initial condition holds, i.e.,

$$T_{0 \rightarrow 1} = \frac{1}{r_{\text{pol}}(1)} \left(\frac{r_{\text{term}}(1) + r_{\text{exc}}(1)}{r_{\text{exc}}(1)} \right).$$

Finally, inserting (29) into (26) results in the analytical expression for $T_{0 \rightarrow N}$,

$$T_{0 \rightarrow N} = \sum_{i=0}^{N-1} \left[\sum_{k=1}^{i+1} \frac{r_{\text{term}}(k) + r_{\text{exc}}(k)}{r_{\text{pol}}(k) \cdot r_{\text{exc}}(k)} \left(\prod_{j=k}^i \frac{r_{\text{pyro}}(j)}{r_{\text{pol}}(j+1)} \right) \right]. \quad (30)$$

Derivation of an analytic solution for polymerization times of homo-polymeric sequences

In case where the sequence to be polymerized is homo-polymeric, e.g. ‘Poly-A’, all rates are uniform, i.e., $r_{\text{pol}}(i) \equiv r_{\text{pol}}, r_{\text{pyro}}(i) \equiv r_{\text{pyro}}, r_{\text{term}}(i) \equiv r_{\text{term}}$ and $r_{\text{exc}}(i) \equiv r_{\text{exc}}$ for any i . Then by exploiting twice the identity

$$\sum_{k=0}^i \left(\frac{r_{\text{pol}}}{r_{\text{pyro}}} \right)^k = \frac{r_{\text{pol}}^{i+1} - r_{\text{pol}}^{i+1}}{(r_{\text{pyro}} - r_{\text{pol}}) \cdot r_{\text{pyro}}^i} \quad (31)$$

the polymerization time from eq. (30) simplifies to

$$\begin{aligned} T_{0 \rightarrow N} &= \left(\frac{r_{\text{term}} + r_{\text{exc}}}{r_{\text{pol}} \cdot r_{\text{exc}}} \right) \sum_{i=0}^{N-1} \left(\frac{r_{\text{pyro}}}{r_{\text{pol}}} \right)^i \sum_{k=0}^i \left(\frac{r_{\text{pol}}}{r_{\text{pyro}}} \right)^k \\ &= \left(\frac{r_{\text{term}} + r_{\text{exc}}}{r_{\text{pol}} \cdot r_{\text{exc}}} \right) \left(\frac{1}{r_{\text{pol}} - r_{\text{pyro}}} \right) \sum_{i=0}^{N-1} \left(r_{\text{pol}} - \left(\frac{r_{\text{pyro}}}{r_{\text{pol}}} \right)^i r_{\text{pyro}} \right) \\ &= \left(\frac{r_{\text{term}} + r_{\text{exc}}}{r_{\text{exc}} \cdot (r_{\text{pol}} - r_{\text{pyro}})^2} \right) \left(r_{\text{pyro}} \left(\left(\frac{r_{\text{pyro}}}{r_{\text{pol}}} \right)^N - N - 1 \right) + r_{\text{pol}} \cdot N \right) \\ T_{0 \rightarrow N} &= \left(\frac{r_{\text{term}} + r_{\text{exc}}}{r_{\text{exc}}} \right) \frac{(r_{\text{pol}} + r_{\text{pyro}})^{N-1} + r_{\text{pol}}^{N-1} \cdot (N-1)}{r_{\text{pol}}^N}, \end{aligned} \quad (32)$$

which is displayed in eq. (16) of the main article.

Determination of the fifty percent inhibitory concentration (IC₅₀)

Starting point for calculating the fifty percent inhibitory concentration (for polymerization of uniform sequences) is equation (19). We set

$$0.5 = \frac{r_{\text{exc}}}{r_{\text{term}} + r_{\text{exc}}} \cdot \frac{r_{\text{pol}}}{r_{\text{pol}}(\phi)} \Leftrightarrow \frac{2}{r_{\text{pol}}(\phi)} = \frac{r_{\text{term}} + r_{\text{exc}}}{r_{\text{exc}} \cdot r_{\text{pol}}}, \quad (33)$$

substitute eqs. (12)–(14) and solve for the NA concentration (that yields 50% inhibition, the IC₅₀ value). After rearranging, we get the quadratic formula

$$a \cdot \text{IC}_{50}^2 + b \cdot \text{IC}_{50} + c = 0 \quad (34)$$

with

$$a = \frac{K_{\text{D,dNTP}}}{K_{\text{D,NA}}} (r_{\text{exc}} + k_{\text{term}}), \quad b = k_{\text{term}} (K_{\text{D,dNTP}} + \text{dNTP})$$

$$c = -r_{\text{exc}} \frac{K_{\text{D,NA}}}{K_{\text{D,dNTP}}} (K_{\text{D,dNTP}} + \text{dNTP})^2,$$

which yields

$$\text{IC}_{50} = \frac{r_{\text{exc}}}{k_{\text{term}} + r_{\text{exc}}} \frac{K_{\text{D,NA}} (K_{\text{D,dNTP}} + [\text{dNTP}])}{K_{\text{D,dNTP}}} \quad (35)$$

Supporting Information

Table S1 Pre-steady state kinetic constants for nucleoside incorporation by wild type HIV-1 reverse transcriptase. Indicated parameters are average values from the respective literature sources. (PDF)

Table S2 Fold change of kinetic parameters for DNA-dependent polymerization in various HIV-1 reverse transcriptase mutants, relative to wildtype RT. $r_{\text{exc}}(\text{wt})$ was set to the value of 0.0016 [1/s] in resting CD4⁺ T-cells for thymidine- and adenosine analogs respectively, see Table S3

References

- Clercq ED (2002) Strategies in the design of antiviral drugs. *Nat Rev Drug Discov* 1: 925–935.
- Tsai CH, Lee PY, Stollar V, Li ML (2006) Antiviral therapy targeting viral polymerase. *Curr Pharm Des* 12: 1339–1355.
- Straus SE, Takiff HE, Seidlin M, Bachrach S, Lininger L, et al. (1984) Suppression of frequently recurring genital herpes. A placebo-controlled double-blind trial of oral acyclovir. *N Engl J Med* 310: 1545–1550.
- Douglas JM, Critchlow C, Benedetti J, Mertz GJ, Connor JD, et al. (1984) A double blind study of oral acyclovir for suppression of recurrences of genital herpes simplex 3 virus infection. *N Engl J Med* 310: 1551–1556.
- Fischl MA, Richman DD, Grieco MH, Gottlieb MS, Volberding PA, et al. (1987) The efficacy of zidovudine (AZT) in the treatment of patients with AIDS and AIDS-related complex. A double-blind, placebo-controlled trial. *N Engl J Med* 317: 185–191.
- Painter GR, Almond MR, Mao S, Liotta DC (2004) Biochemical and mechanistic basis for the activity of nucleoside analogue inhibitors of HIV reverse transcriptase. *Curr Top Med Chem* 4: 1035–1044.
- von Kleist M, Menz S, Huisinga W (2010) Drug-class specific impact of antivirals on the reproductive capacity of HIV. *PLoS Comput Biol* 6: e1000720.
- Johnson AA, Ray AS, Hanes J, Suo Z, Colacino JM, et al. (2001) Toxicity of antiviral nucleoside analogs and the human mitochondrial DNA polymerase. *J Biol Chem* 276: 40847–40857.
- Lewis W, Day BJ, Copeland WC (2003) Mitochondrial toxicity of NRTI antiviral drugs: an integrated cellular perspective. *Nat Rev Drug Discov* 2: 812–822.
- Brown JA, Pack LR, Fowler JD, Suo Z (2011) Pre-steady-state kinetic analysis of the incorporation of anti-HIV nucleoside analogs catalyzed by human x- and y-family DNA polymerases. *Antimicrob Agents Chemother* 55: 276–283.
- Hanes JW, Zhu Y, Parris DS, Johnson KA (2007) Enzymatic therapeutic index of acyclovir. Viral versus human polymerase gamma specificity. *J Biol Chem* 282: 25159–25167.
- Memendez-Arias L (2008) Mechanisms of resistance to nucleoside analogue inhibitors of HIV-1 reverse transcriptase. *Virus Res* 134: 124–146.
- Goldschmidt V, Marquet R (2004) Primer unblocking by HIV-1 reverse transcriptase and resistance to nucleoside RT inhibitors (NRTIs). *Int J Biochem Cell Biol* 36: 1687–1705.
- Goody RS, Miller B, Restle T (1991) Factors contributing to the inhibition of HIV reverse transcriptase by chain-terminating nucleotides in vitro and in vivo. *FEBS Lett* 291: 1–5.
- Meyer PR, Matsuura SE, Mian AM, So AG, Scott WA (1999) A mechanism of AZT resistance: an increase in nucleotide-dependent primer unblocking by mutant HIV-1 reverse transcriptase. *Mol Cell* 4: 35–43.
- Boyer PL, Sarafianos SG, Arnold E, Hughes SH (2001) Selective excision of AZTMP by drug-resistant human immunodeficiency virus reverse transcriptase. *J Virol* 75: 4832–4842.
- Ray AS, Murakami E, Basavapathruni A, Vaccaro JA, Ulrich D, et al. (2003) Probing the molecular mechanisms of AZT drug resistance mediated by HIV-1 reverse transcriptase using a transient kinetic analysis. *Biochemistry* 42: 8831–8841.

(supplementary material) and eq. (18) (main article) and to the value of 0.00053 [1/s] for guanine- and cytosine analogs, see [76].
^b excision of TFV-TP from terminated templates was assumed to be 100%, 50%, 100% and 40% of the wild type excision rate for the M184V, the K65R, the Q151M and the K65R/M184V mutant, see [77].
[§] CBV-TP excision in the Q151M mutant was set to 5300% of wild type excision, see [76].
[¶] D4T-TP excision in the M184V mutant was set to 83% of the wild type excision, assuming a similar effect of M184V on D4T-TP and AZT-TP [77]. If no other information was available, excisions of nucleoside analogs in the mutant enzymes were assumed to be equal to the wild type excision rate.
^{*} Q151Mc denotes the ‘A62V/V75I/F77L/F116Y/Q151M’ mutant.
^{**} 4-TAM denotes the ‘D67N/K70R/T215Y/K219Q’ mutant.
[†] set to the value of 1, because of insufficient information.
[‡] set equal to the rate in Q151Mc. (PDF)

Table S3 Pre-steady state kinetic constants for AZT excision by HIV-1 reverse transcriptase wildtype and ‘D67N/K70R/T215Y/K219Q’ mutant. * Parameter could not be accurately determined in the respective study [17]. (PDF)

Table S4 Pre-steady state kinetic constants for nucleoside incorporation by human mitochondrial polymerase-γ. * r_{pyro} was set to value zero because of insufficient information. (PDF)

Text S1 The supplementary text contains the modelling required to compute the probability to successfully complete reverse transcription (RT) in HIV-1, based on the parameters presented in the main manuscript. (PDF)

Acknowledgments

MvK and CS acknowledge fruitful discussions with Dr. Michael Wulkow, CiT (Rastede, Germany).

Author Contributions

Conceived and designed the experiments: MvK PM RM CS. Performed the experiments: MvK. Analyzed the data: MvK RM PM CS. Wrote the paper: MvK RM.

18. Krebs R, Immendorfer U, Thrall SH, Whrl BM, Goody RS (1997) Single-step kinetics of HIV-1 reverse transcriptase mutants responsible for virus resistance to nucleoside inhibitors zidovudine and 3-TC. *Biochemistry* 36: 10292–10300.
19. Khalil S, Monaco JM, Armaou A (2010) Development of a stochastic model for the efficacy of NRTIs using known mechanisms of action. *J Theor Biol* 265: 704–717.
20. Buckheit RW (2004) Understanding HIV resistance, fitness, replication capacity and compensation: targeting viral fitness as a therapeutic strategy. *Expert Opin Investig Drugs* 13: 933–958.
21. Martinez-Picado J, Martinez MA (2008) HIV-1 reverse transcriptase inhibitor resistance mutations and fitness: a view from the clinic and ex vivo. *Virus Res* 134: 104–123.
22. Bonhoeffer S, Chappey C, Parkin NT, Whitcomb JM, Petropoulos CJ (2004) Evidence for positive epistasis in hiv-1. *Science* 306: 1547–1550.
23. Martnez JP, Bocharov G, Ignatovich A, Reiter J, Dittmar RT, et al. (2011) Fitness ranking of individual mutants drives patterns of epistatic interactions in hiv-1. *PLoS One* 6: e18375.
24. D'Abramo CM, Cellai L, Gtce M (2004) Excision of incorporated nucleotide analogue chain-terminators can diminish their inhibitory effects on viral RNA-dependent RNA polymerases. *J Mol Biol* 337: 1–14.
25. Deval J, Powdermill MH, D'Abramo CM, Cellai L, Gtce M (2007) Pyrophosphorylation of nonobligate chain terminators by hepatitis C virus NS5B polymerase. *Antimicrob Agents Chemother* 51: 2920–2928.
26. Urban S, Urban S, Fischer KP, Tyrrell DL (2001) Efficient pyrophosphorylation by a hepatitis b virus polymerase may be a primer-unblocking mechanism. *Proc Natl Acad Sci U S A* 98: 4984–4989.
27. von Kleist M, Menz S, Stocker H, Arasteh K, Schütte C, et al. (2011) HIV quasispecies dynamics during pro-active treatment switching: Impact on multi-drug resistance and resistance archiving in latent reservoirs. *PLoS One* 6: e18204.
28. Klatzmann D, Barr-Sinoussi F, Nugeyre MT, Danquet C, Vilmer E, et al. (1984) Selective tropism of lymphadenopathy associated virus (LAV) for helper-inducer T lymphocytes. *Science* 225: 59–63.
29. Koenig S, Gendelman HE, Orenstein JM, Canto MCD, Pezeskhpour GH, et al. (1986) Detection of AIDS virus in macrophages in brain tissue from AIDS patients with encephalopathy. *Science* 233: 1089–1093.
30. Patterson S, Rae A, Hockey N, Gilmour J, Gotch F (2001) Plasmacytoid dendritic cells are highly susceptible to human immunodeficiency virus type 1 infection and release infectious virus. *J Virol* 75: 6710–6713.
31. Valentin A, Rosati M, Patenaude DJ, Hatzakis A, Kostrikis LG, et al. (2002) Persistent HIV-1 infection of natural killer cells in patients receiving highly active antiretroviral therapy. *Proc Natl Acad Sci U S A* 99: 7015–7020.
32. Takahashi K, Wesselingh SL, Griffin DE, McArthur JC, Johnson RT, et al. (1996) Localization of HIV-1 in human brain using polymerase chain reaction/in situ hybridization and immunocytochemistry. *Ann Neurol* 39: 705–711.
33. Kepler TB, Perelson AS (1998) Drug concentration heterogeneity facilitates the evolution of drug resistance. *Proc Natl Acad Sci U S A* 95: 11514–11519.
34. Smith AJ, Scott WA (2006) The influence of natural substrates and inhibitors on the nucleotide-dependent excision activity of HIV-1 reverse transcriptase in the infected cell. *Curr Pharm Des* 12: 1827–1841.
35. Smith AJ, Meyer PR, Asthana D, Ashman MR, Scott WA (2005) Intracellular substrates for the primer-unblocking reaction by human immunodeficiency virus type 1 reverse transcriptase: detection and quantitation in extracts from quiescent- and activated-lymphocyte subpopulations. *Antimicrob Agents Chemother* 49: 1761–1769.
36. Traut TW (1994) Physiological concentrations of purines and pyrimidines. *Mol Cell Biochem* 140: 1–22.
37. Goday A, Simmonds HA, Webster DR, Levinsky RJ, Watson AR, et al. (1983) Importance of platelet-free preparations for evaluating lymphocyte nucleotide levels in inherited or acquired immunodeficiency syndromes. *Clin Sci (Lond)* 65: 635–643.
38. Goday A, Webster DR, Simmonds HA, Levinsky RJ, Perrett D, et al. (1984) Nu1-cleotide levels in peripheral blood mononuclear cells of immunodeficient children: problems of measurement. *Adv Exp Med Biol* 165 Pt B: 179–182.
39. Tu X, Das K, Han Q, Bauman JD, Clark AD, et al. (2010) Structural basis of HIV-1 resistance to AZT by excision. *Nat Struct Mol Biol* 17: 1202–1209.
40. Stanford University (2011) HIV drug resistance database. URL <http://hivdb.stanford.edu/pages/phenoSummary/Pheno.NRTI.Simple.html>.
41. Frankel FA, Invernizzi CF, Oliveira M, Wainberg MA (2007) Diminished efficiency of HIV-1 reverse transcriptase containing the K65R and M184V drug resistance mutations. *AIDS* 21: 665–675.
42. Svedhem V, Lindkvist A, Lidman K, Snnerborg A (2002) Persistence of earlier HIV-1 drug resistance mutations at new treatment failure. *J Med Virol* 68: 473–478.
43. Petropoulos CJ, Parkin NT, Limoli KL, Lie YS, Wrin T, et al. (2000) A novel phenotypic drug susceptibility assay for human immunodeficiency virus type 1. *Antimicrob Agents Chemother* 44: 920–928.
44. Kakuda TN (2000) Pharmacology of nucleoside and nucleotide reverse transcriptase inhibitor-induced mitochondrial toxicity. *Clin Ther* 22: 685–708.
45. Aquaro S, Perno CF, Balestra E, Balzarini J, Cenci A, et al. (1997) Inhibition of replication of HIV in primary monocyte/macrophages by different antiviral drugs and comparative efficacy in lymphocytes. *J Leukoc Biol* 62: 138–143.
46. Kellam P, Boucher CA, Larder BA (1992) Fifth mutation in human immunodeficiency virus type 1 reverse transcriptase contributes to the development of high-level resistance to zidovudine. *Proc Natl Acad Sci U S A* 89: 1934–1938.
47. Byrnes VW, Emini EA, Schleif WA, Condra JH, Schneider CL, et al. (1994) Susceptibilities of human immunodeficiency virus type 1 enzyme and viral variants expressing multiple resistance-engendering amino acid substitutions to reserve transcriptase inhibitors. *Antimicrob Agents Chemother* 38: 1404–1407.
48. Garca-Lerma JG, Aung W, Cong M, Zheng Q, Youngprajoi AS, et al. (2011) Natural substrate concentrations can modulate the prophylactic efficacy of nucleotide hiv reverse transcriptase inhibitors. *J Virol* 85: 6610–6617.
49. Perez-Bercoff D, Wurtzer S, Compain S, Bench H, Clavel F (2007) Human immunodeficiency virus type 1: resistance to nucleoside analogues and replicative capacity in primary human macrophages. *J Virol* 81: 4540–4550.
50. Buzon MJ, Massanella M, Llibre JM, Esteve A, Dahl V, et al. (2010) HIV-1 replication and immune dynamics are affected by raltegravir intensification of HAART-suppressed subjects. *Nat Med* 16: 460–465.
51. Brennan TP, Woods JO, Sedaghat AR, Siliciano JD, Siliciano RF, et al. (2009) Analysis of human immunodeficiency virus type 1 viremia and provirus in resting CD4+ T cells reveals a novel source of residual viremia in patients on antiretroviral therapy. *J Virol* 83: 8470–8481.
52. Elena SF, Sol RV, Sardany J (2010) Simple genomes, complex interactions: epistasis in rna virus. *Chaos* 20: 026106.
53. von Kleist M, Huisinga W (2009) Pharmacokinetic-pharmacodynamic relationship of NRTIs and its connection to viral escape: an example based on zidovudine. *Eur J Pharm Sci* 36: 532–543.
54. Lavie A, Schlichting I, Vetter IR, Konrad M, Reinstein J, et al. (1997) The bottleneck in AZT activation. *Nat Med* 3: 922–924.
55. Lavie A, Su Y, Ghassemi M, Novak RM, Caffrey M, et al. (2008) Restoration of the antiviral activity of 3'-azido-3'-deoxythymidine (AZT) against AZT-resistant human immunodeficiency virus by delivery of engineered thymidylate kinase to T cells. *J Gen Virol* 89: 1672–1679.
56. Ray AS (2005) Intracellular interactions between nucleos(t)ide inhibitors of HIV reverse transcriptase. *AIDS Rev* 7: 113–125.
57. McKee EE, Bentley AT, Hatch M, Gingerich J, Susan-Resiga D (2004) Phosphorylation of thymidine and AZT in heart mitochondria: elucidation of a novel mechanism of AZT cardiotoxicity. *Cardiovasc Toxicol* 4: 155–167.
58. Bradshaw PC, Li J, Samuels DC (2005) A computational model of mitochondrial AZT metabolism. *Biochem J* 392: 363–373.
59. Freisz S, Bec G, Radi M, Wolff P, Crespan E, et al. (2010) Crystal structure of HIV-1 reverse transcriptase bound to a non-nucleoside inhibitor with a novel mechanism of action. *Angew Chem Int Ed Engl* 49: 1805–1808.
60. Radi M, Maga G, Alongi M, Angeli L, Samuele A, et al. (2009) Discovery of chiral cyclopropyl dihydro-alkylthio-benzyl-oxopyrimidine (S-DABO) derivatives as potent HIV-1 reverse transcriptase inhibitors with high activity against clinically relevant mutants. *J Med Chem* 52: 840–851.
61. Jochmans D, Deval J, Kesteleyn B, Marck HV, Bettens E, et al. (2006) Indolopyridones inhibit human immunodeficiency virus reverse transcriptase with a novel mechanism of action. *J Virol* 80: 12283–12292.
62. Liu S, Harada BT, Miller JT, Grice SFJL, Zhuang X (2010) Initiation complex dynamics direct the transitions between distinct phases of early hiv reverse transcription. *Nat Struct Mol Biol* 17: 1453–1460.
63. Liu S, Abbondanzieri EA, Rausch JW, Grice SFJL, Zhuang X (2008) Slide into action: dynamic shuttling of hiv reverse transcriptase on nucleic acid substrates. *Science* 322: 1092–1097.
64. Thomas DC, Voronin YA, Nikolenko GN, Chen J, Hu WS, et al. (2007) Determination of the ex vivo rates of human immunodeficiency virus type 1 reverse transcription by using novel strand-specific amplification analysis. *J Virol* 81: 4798–4807.
65. Shen L, Peterson S, Sedaghat AR, McMahon MA, Callender M, et al. (2008) Dose-response curve slope sets class-specific limits on inhibitory potential of anti-HIV drugs. *Nat Med* 14: 762–766.
66. Shen L, Rabi SA, Sedaghat AR, Shan L, Lai J, et al. (2011) A critical subset model provides a conceptual basis for the high antiviral activity of major hiv drugs. *Sci Transl Med* 3: 91ra63.
67. Xia Q, Radzio J, Anderson KS, Sluis-Cremer N (2007) Probing nonnucleoside inhibitor-induced active-site distortion in HIV-1 reverse transcriptase by transient kinetic analyses. *Protein Sci* 16: 1728–1737.
68. Sluis-Cremer N, Tachedjian G (2008) Mechanisms of inhibition of HIV replication by non-nucleoside reverse transcriptase inhibitors. *Virus Res* 134: 147–156.
69. Karlin S, Taylor HM (1975) A first course in stochastic processes. London: Academic Press.
70. Norris JR (1998) Markov chains. Cambridge, UK: Cambridge University Press.
71. Anderson PL, Zheng JH, King T, Bushman LR, Predhomme J, et al. (2007) Concentrations of zidovudine- and lamivudine-triphosphate according to cell type in HIV-seronegative adults. *AIDS* 21: 1849–1854.
72. Chapman EH, Kurec AS, Davey FR (1981) Cell volumes of normal and malignant mononuclear cells. *J Clin Pathol* 34: 1083–1090.
73. Kiser JJ, Aquilante CL, Anderson PL, King TM, Carten ML, et al. (2008) Clinical and genetic determinants of intracellular tenofovir diphosphate concentrations in HIV-infected patients. *J Acquir Immune Defic Syndr* 47: 298–303.
74. Anderson PL, Kiser JJ, Gardner EM, Rower JE, Meditz A, et al. (2011) Pharmacological considerations for tenofovir and emtricitabine to prevent HIV infection. *J Antimicrob Chemother* 66: 240–250.

75. Becher F, Landman R, Mboup S, Kane CNT, Canestri A, et al. (2004) Monitoring of didanosine and stavudine intracellular triphosphorylated anabolite concentrations in HIV-infected patients. *AIDS* 18: 181–187.
76. Ray AS, Basavapathruni A, Anderson KS (2002) Mechanistic studies to understand the progressive development of resistance in human immunodeficiency virus type 1 reverse transcriptase to abacavir. *J Biol Chem* 277: 40479–40490.
77. Ly JK, Margot NA, MacArthur HL, Hung M, Miller MD, et al. (2007) The balance between NRTI discrimination and excision drives the susceptibility of HIV-1 RT mutants K65R, M184V and K65R+M184V. *Antivir Chem Chemother* 18: 307–316.